Cell Reports

Article

Impaired oxysterol-liver X receptor signaling underlies aberrant cortical neurogenesis in a stem cell model of neurodevelopmental disorder

Graphical abstract

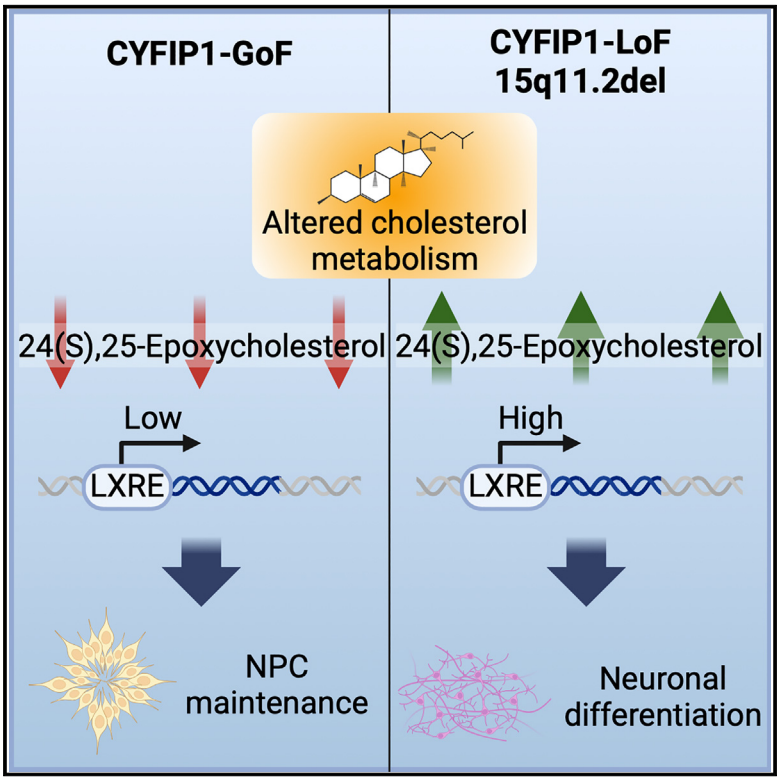

Authors

Daniel Cabezas De La Fuente, Claudia Tamburini, Emily Stonelake, ..., David E.J. Linden, Andrew Pocklington, Meng Li

Correspondence

lim26@cf.ac.uk

In brief

De La Fuente et al. reveal a regulatory role for CYFIP1 in cholesterol metabolism and oxysterol levels. CYFIP1 gain and loss of function and 15q11.2 deletion led to disturbed cortical neurogenesis, a pathological event mediated by altered levels of oxysterols and their interaction with the liver X receptor.

Highlights

- CYFIP1 safeguards cortical neurogenesis during development
- Gain and loss of CYFIP1 function leads to disturbed cholesterol metabolism
- 24S,25-epoxycholesterol restores delayed neurogenesis caused by elevated CYFIP1
- CYFIP1 regulation of neurogenesis is mediated through oxysterol signaling via LXR

De La Fuente et al., 2024, Cell Reports *43*, 113946
March 26, 2024
https://doi.org/10.1016/j.celrep.2024.113946

CellPress

Cell Reports

CellPress
OPEN ACCESS

Article

Impaired oxysterol-liver X receptor signaling underlies aberrant cortical neurogenesis in a stem cell model of neurodevelopmental disorder

Daniel Cabezas De La Fuente,[1,7] Claudia Tamburini,[1,7] Emily Stonelake,[5] Robert Andrews,[3] Jeremy Hall,[1,2] Michael J. Owen,[1,2] David E.J. Linden,[1,2,6] Andrew Pocklington,[2] and Meng Li[1,2,4,8,*]

[1]Neuroscience and Mental Health Innovation Institute, Cardiff University, Cardiff, UK
[2]Division of Psychiatry and Clinical Neuroscience, Cardiff University, Cardiff, UK
[3]Division of Infection and Immunity, School of Medicine, Cardiff University, Cardiff, UK
[4]School of Bioscience, Cardiff University, Cardiff, UK
[5]Swansea University, University Medical School, Swansea, UK
[6]School for Mental Health and Neuroscience, Faculty of Health, Medicine and Life Sciences, Maastricht University, Maastricht, the Netherlands
[7]These authors contributed equally
[8]Lead contact
*Correspondence: lim26@cf.ac.uk
https://doi.org/10.1016/j.celrep.2024.113946

SUMMARY

The mechanisms by which genomic risks contribute to the onset of neuropsychiatric conditions remain a key challenge and a prerequisite for successful development of effective therapies. 15q11.2 copy number variation (CNV) containing the *CYFIP1* gene is associated with autism and schizophrenia. Using stem cell models, we show that 15q11.2 deletion (15q11.2del) and CYFIP1 loss of function (CYFIP1-LoF) lead to premature neuronal differentiation, while CYFIP1 gain of function (CYFIP1-GoF) favors neural progenitor maintenance. CYFIP1 dosage changes led to dysregulated cholesterol metabolism and altered levels of 24S,25-epoxycholesterol, which can mimic the 15q11.2del and CYFIP1-LoF phenotypes by promoting cortical neuronal differentiation and can restore the impaired neuronal differentiation of CYFIP1-GoF neural progenitors. Moreover, the neurogenic activity of 24S,25-epoxycholesterol is lost following genetic deletion of liver X receptor (*LXRβ*), while compound deletion of LXRβ in *CYFIP1*$^{-/-}$ background rescued their premature neurogenesis. This work delineates LXR-mediated oxysterol regulation of neurogenesis as a pathological mechanism in neural cells carrying 15q11.2 CNV and provides a potential target for therapeutic strategies for associated disorders.

INTRODUCTION

Neurodevelopmental disorders, such as autism and schizophrenia, are believed to originate during early brain development with shared genetic etiology.[1] Copy number variations (CNVs) at the chromosomal locus 15q11.2 (BP1-BP2) have been found by several genome-wide association studies to be significantly linked to an increased risk of developing these disorders.[2–6] In addition to psychiatric features, the clinical phenotype of 15q11.2 CNV carriers frequently includes other traits, such as developmental delay, seizures, and motor coordination problems.[7] The 15q11.2 region spans approximately 500 kb and contains four genes encoding CYFIP1, NIPA1, NIPA2, and TUBGCP5.[8] CYFIP1 (cytoplasmic FMR1 interacting protein) is considered to be the strongest candidate underlying the link between 15q11.2 CNVs and psychiatric illness due to its functional association with the fragile X mental retardation protein (FMRP).[9,10] In addition to regulating mRNA translation together with FMRP, CYFIP1 is also part of the WAVE complex that controls actin polymerization.[11] CYFIP1 is enriched in dendritic spines, and alterations in its level in rodent primary cultures and genetic mouse models affect dendritic morphology and synaptic function,[12–15] disrupt adult neurogenesis,[16,17] and cause white matter changes.[18,19]

While previous studies into CYFIP1 mostly focused on the adult brain, transcript levels of *CYFIP1* are highest in the first trimester of human brain development (Human Brain Transcriptone: http://hbatlas.org/pages/hbtd), and *in situ* hybridization of fetal mouse brain shows *Cyfip1* RNA concentrated in the ventricular zone and sub-ventricular zone (Eurexpress: http://www.eurexpress.org). Consistent with its early expression profile, shRNA knockdown of CYFIP1 in human embryonic stem cell (hESC)-derived neural progenitors disrupts their polarity, while electroporation of shRNA-*Cyfip1* into the developing mouse cortex affects cortical progenitor migration.[20] Neuroepithelial polarity and progenitor migration are intricately associated with neural

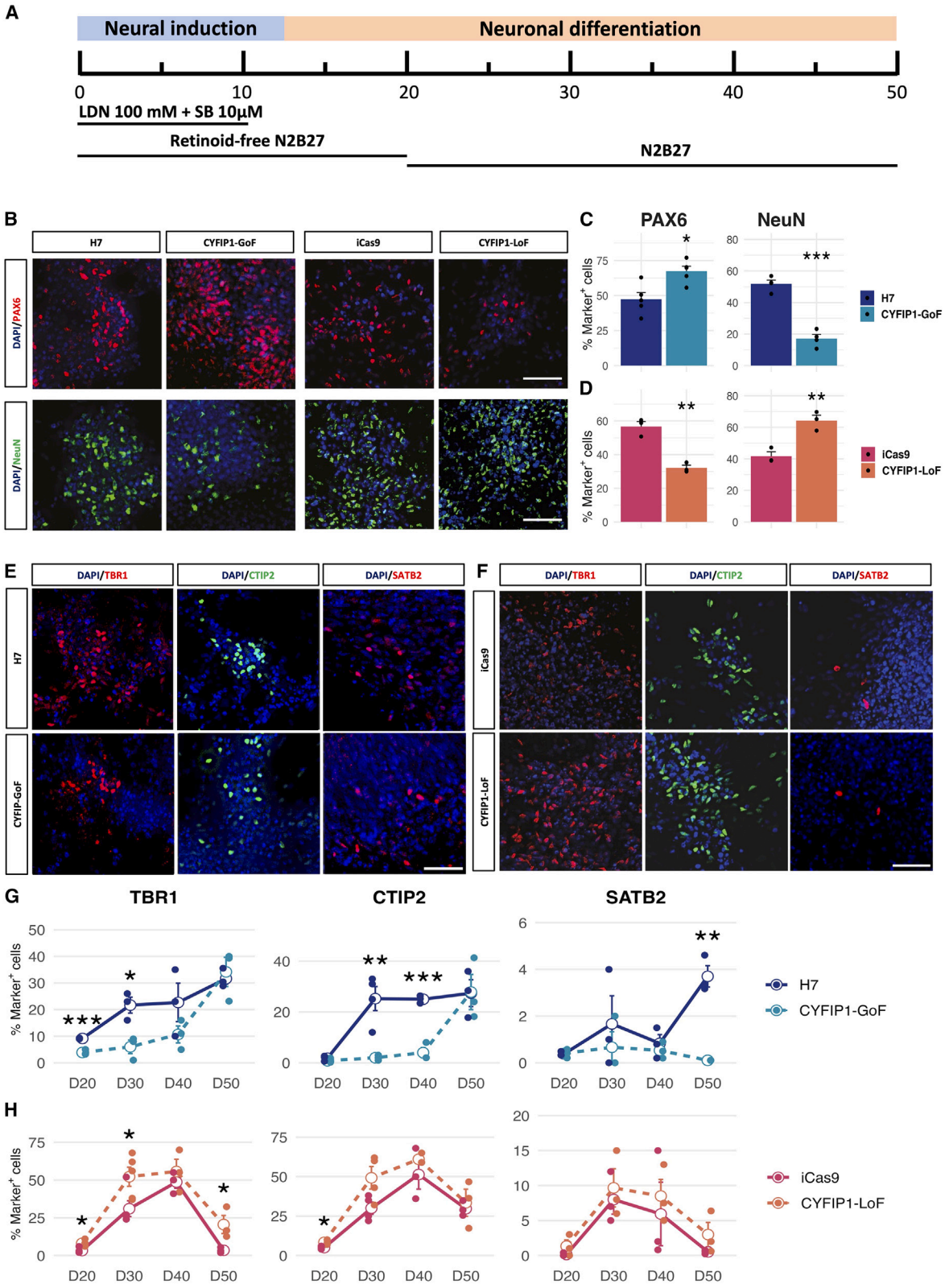

(legend on next page)

progenitor cell (NPC) division and neurogenesis. The above findings thus raise the question of whether CYFIP1 deficiency leads to aberrant progenitor proliferation and neuronal differentiation. Moreover, whether an increase in CYFIP1 protein level, as in 15q11.2 duplication (15q11.2dup), affects cortical neural induction and neuronal function remains unknown.

Using transgene expression and CRISPR-Cas9-assisted genome editing of *CYFIP1* in hESCs and patient-derived induced pluripotent stem cells (iPSCs) harboring 15q11.2 chromosomal deletions (15q11.2del iPSCs), we find that gain and loss of CYFIP1 disturb cortical NPC proliferation and differentiation with opposing directions of effect. Defects caused by CYFIP1 deficiency were mirrored by 15q11.2del iPSC-derived neural cells. Moreover, we provide unexpected evidence that CYFIP1-dependent neurogenesis is regulated through controlling biosynthesis and metabolism of oxysterols, which directly affects neurogenic activity of NPCs via the liver X receptor (LXR) signaling. Thus, our study identifies CYFIP1 as a regulator for cortical neurogenesis and provides mechanistic insight into the causes of the neurodevelopmental impairment in 15q11.2 CNV carriers and potential therapeutic targets.

RESULTS

Gain and loss of CYFIP1 led to altered neuronal differentiation kinetics

To mimic CYFIP1 dosage change in 15q11.2del and 15q11.2dup, we generated stable, clonal lines of hESCs that were either deficient in CYFIP1 expression (CYFIP1 loss-of-function, CYFIP1-LoF) or carry a CYFIP1 transgene (CYFIP1 gain-of-function, CYFIP1-GoF). The CYFIP1-LoF lines were generated by CRISPR-Cas9-assisted genome editing in the iCas9 background,[21] while the CYFIP1-GoF cells were of H7 origin and ubiquitously express human CYFIP1 driven by the CAG promoter (for details, see STAR methods and Figures S1A–S1F). The CYFIP1-GoF lines used in this study (#3 and #5) exhibited approximately 2-fold increase of CYFIP1 (Figure S1B–S1D), while CYFIP1-LoF lines showed ~5% (clone #31) and 40% (clone #41) CYFP1 protein level of their isogenic wild-type control cells, respectively (Figure S1G).

CYFIP1 transcript levels are highest in the first trimester of human telencephalic development (http://hbatlas.org/pages/hbtd). We therefore investigated the effect of CYFIP1 dosage change on cortical neural differentiation of CYFIP1-LoF and CYFIP1-GoF hESCs (Figure 1A). At day 15 (d15), the CYFIP1-GoF and CYFIP1-LoF cultures contained a similar number of FOXG1$^+$ and PAX6$^+$ forebrain progenitors compared to their respective isogenic control cultures (Figure S2), suggesting a normal cortical neural induction from human pluripotent stem cells (hPSCs). However, at day 35 (d35) when neurons are actively produced, we detected a marked reduction of NeuN$^+$ neurons in CYFIP1-GoF cultures compared to the isogenic controls (Figures 1B and 1C). The CYFIP1-LoF cultures showed the opposite phenomenon with a significant increase of NeuN$^+$ cells compared to their control cultures (Figures 1C and 1D).

We next broadened the analysis time window from d20 till d50 of differentiation cultures and examined typical markers representing different layers of cortical neurons. CYFIP1-GoF cultures contained a lower percentage of TBR1$^+$ and CTIP2$^+$ cells compared to their respective isogenic controls between d20 and d40 but caught up by d50 (Figures 1E and 1G). Conversely, the percentage of these neuronal subtypes was generally higher in the CYFIP1-LoF population than the isogenic controls (Figures 1F and 1H). SATB2 is expressed in the upper layer and a subset of CTIP2$^+$ cortical neurons.[22] SATB2$^+$ neurons largely mirrored the trend for deep-layer markers but were detected in low numbers with statistical significance only reached for CYFIP1-GoF at d50.

The opposite trend of change in neural progenitor and neuronal numbers was supported by western blot analysis using independent preparations of cortical differentiation. We detected an increase in the total protein levels of TBR1,CTIP2, and NeuN and a concurrent decrease of PAX6 in d30 CYFIP1-LoF cells compared to the iCas9 isogenic controls, with changes in PAX6 also observed at d15 (Figures S2D and S2E). In contrast, an opposite trend of change was observed in CYFIP1-GoF samples compared to H7 controls. Together, these experiments demonstrate that elevated levels of CYFIP1 led to a delayed neuronal production, while CYFIP1-deficiency results in precocious neuronal differentiation.

CYFIP1 dosage change affects neurogenesis rate of cortical progenitors

Given the altered neuronal differentiation kinetics observed above, we next carried out a pulse-chase EdU incorporation assay at d30 followed by double EdU/NeuN antibody staining 5 days later to determine the relative neuronal birth rate by CYFIP1-GoF and -LoF neural progenitors (Figure 2). We found that the CYFIP1-GoF cultures contained fewer EdU-retaining NeuN$^+$ neurons than the isogenic control cultures (Figures 2A and 2B). In contrast, there were more EdU-retaining NeuN$^+$ neurons in CYFIP1-LoF cultures than in the respective controls (Figures 2A–2C), suggesting that CYFIP1 levels regulate the rate of neurogenesis in these cortical progenitors.

Consistent with the above findings, flow-cytometry-based cell cycle analysis revealed a higher percentage of G2/M-phase progenitors in CYFIP1-GoF cultures than the controls (GoF,

Figure 1. Gain and loss of CYFIP1 affect temporal kinetics of neuronal differentiation

(A) Outline of the cortical differentiation paradigm.

(B) Immunostaining for PAX6 (red) and NeuN (green) for CYFIP1-GoF, CYFIP1-LoF, and their respective isogenic controls at d35 of differentiation.

(C and D) Quantification of PAX6$^+$ and NeuN$^+$ cells shown in (B).

(E and F) d20–d50 cortical cultures were immunostained for cortical neuronal markers TBR1 (red), CTIP2 (green), and SATB2 (red); shown are representative images of d30 staining.

(G and H) Quantification of TBR1$^+$, CTIP2$^+$, and SATB2$^+$ of d20–d50 cortical cultures, respectively. Data presented are mean ± SEM of at least three biological replicates indicated in dots and Table S10; groups were compared by Student's t test between the CYFIP1-manipulated vs. isogenic control at each time point (*$p < 0.05$; **$p < 0.01$; ***$p < 0.001$). Nuclei were counterstained with DAPI (blue). Scale bars: 50 μm.

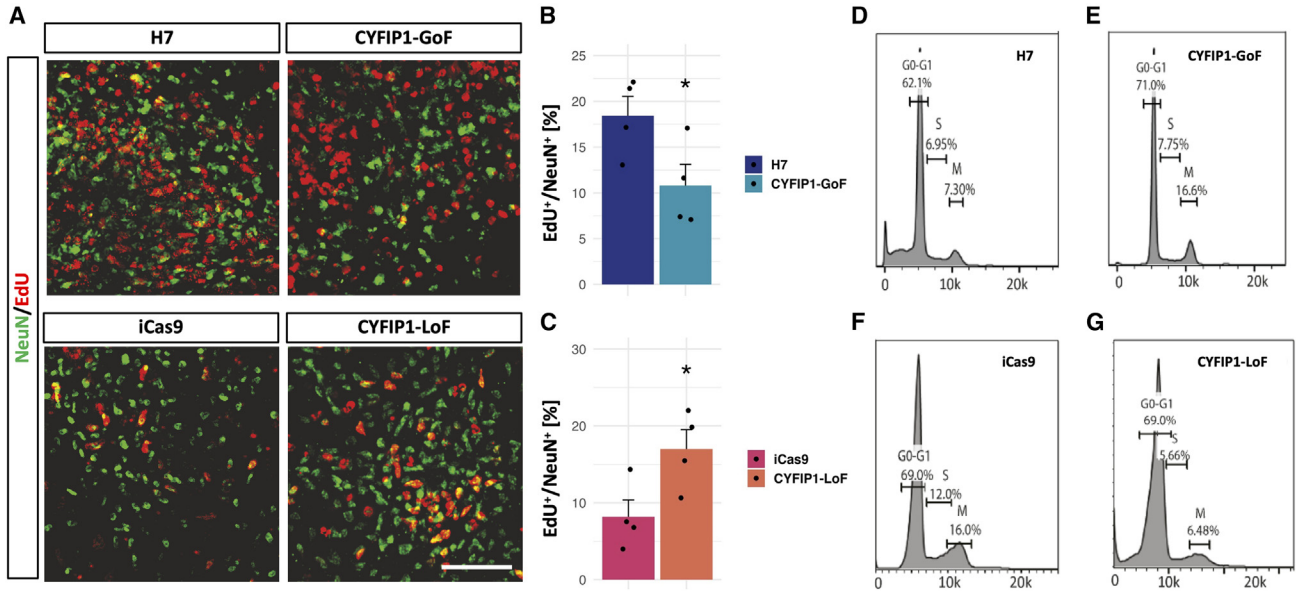

Figure 2. CYFIP1 dosage change affects NPC cell-cycle profile

(A) Representative images of cells labeled with EdU (red) and NeuN (green) at d35. D30 cultures were incubated with EdU for 2 h and co-immunostained 5 days later for EdU and NeuN. Scale bar: 50 μm.

(B and C) Quantification of EdU-retaining cells in NeuN$^+$ neurons. Data presented are mean ± SEM from four biological replicates. Student's t test, n = 4, *p < 0.05.

(D and G) Representative histograms of a flow-cytometry-based cell-cycle analysis on d20 cultures.

16.13% ± 3.3%; H7, 5.53% ± 1.36%, n = 3, p < 0.005, Figures 2D and 2E and Table S1). In contrast, a reduced number of S-phase cells were detected in the CYFIP1-LoF cultures compared to the isogenic controls (LoF, 3.91% ± 1.97%, iCas9, 8.39% ± 3.07%, n = 4, p < 0.05, Figures 2F and 2G and Table S1). This change in cell cycle profile of CYFIP1-LoF cultures was also associated with a reduction in the number of cells positive for the proliferation marker Ki67 and a concurrent increase in cells expressing the cell cycle regulator P27^{kip1} (Figure S3), which can promote neuronal differentiation in the cerebral cortex.[23] These observations suggest that a tight regulation of CYFIP1 level is essential for normal cortical NPC division and neurogenesis.

Genome-wide transcriptome studies confirm altered neural developmental kinetics and reveal disrupted cholesterol biosynthesis and metabolism

In order to gain a deeper understanding of the cellular mechanisms and pathways disrupted by CYFIP1 dosage change, we performed RNA sequencing (RNA-seq) of CYFIP1-GoF and CYFIP1-LoF and their respective parental control cells at three time points of cortical neural differentiation, which represent an early NPC (NPC1, d10), peak NPC and onset of neurogenesis (NPC2, d20), and neuronal rich (neuronal, d40) stages, respectively (Figure 3A). Principal component analysis revealed a clear differentiation stage (PC1)- and genotype (PC2)-dependent separation in both the CYFYP1-GoF and CYFIP1-LoF datasets (Figures S4A and S4B). Pronounced CYFIP1-led transcriptomic changes were evident at NPC2 and neuronal stages, which reflect the neurogenesis defect observed from this stage onward. Among the differentially expressed genes (DEGs) between cells with CYFIP1 dosage change and their isogenic controls include transcription factors and signaling molecules defining neural progenitor identity or playing important roles in cortical development, such as *PAX6*, *GLI3*, *EMX1*, and *EMX2*,[24] *frizzled receptors* (*FZDs*), *LHX2*, *SALL1*,[25] *FAM107A*,[26] and *dopachrome tautomerase* (*DCT*)[27] (Figures 3B, 3C, S4C, and S4D and Tables S2 and S3). Significant changes were also detected for genes associated with neuronal differentiation and synapse formation, such as *doublecortin* (*DCX*), *synaptotagmins* (*SYT1* and *SYT2*),[28] *GFRA1*,[29] *PTN*,[30] and *DLG4* (*PSD95*) (Figures 3B, 3C, S4C, and S4D; Tables S2 and S3). Many DEGs showed the opposite direction of change in CYFIP1-GoF and CYFIP1-LoF samples (Figures 3B and 3C).

To reveal CYFIP1-regulated biological processes and molecular pathways, we analyzed CYFIP1-GoF and CYFIP1-LoF protein-coding DEGs separately at each developmental stage to identify enriched gene ontology (GO) terms. GO terms significantly over-represented (Benjamini-Hochberg-corrected p < 0.05) among DEGs were primarily linked to the regulation of central nervous system development (Figures 3D and 3E), reflecting the findings of altered differentiation kinetic of NPCs and their direction of change. For example, "neural precursor cell proliferation" was among the most significant terms in CYFIP1-GoF samples, while one of the highest in the list of GO terms associated with CYFIP1-LoF was "cell differentiation." Terms relating to microtubule cytoskeleton organization and synaptic assembly were also significantly enriched, indicating that our results are in line with previously reported functions of CYFIP1 (Figures 3D and 3E and Tables S4 and S5). Unexpectedly, this analysis identified the presence of significant alterations of cholesterol biosynthesis and sterol response in both CYFIP1-GoF and CYFIP1-LoF samples, as demonstrated by differential

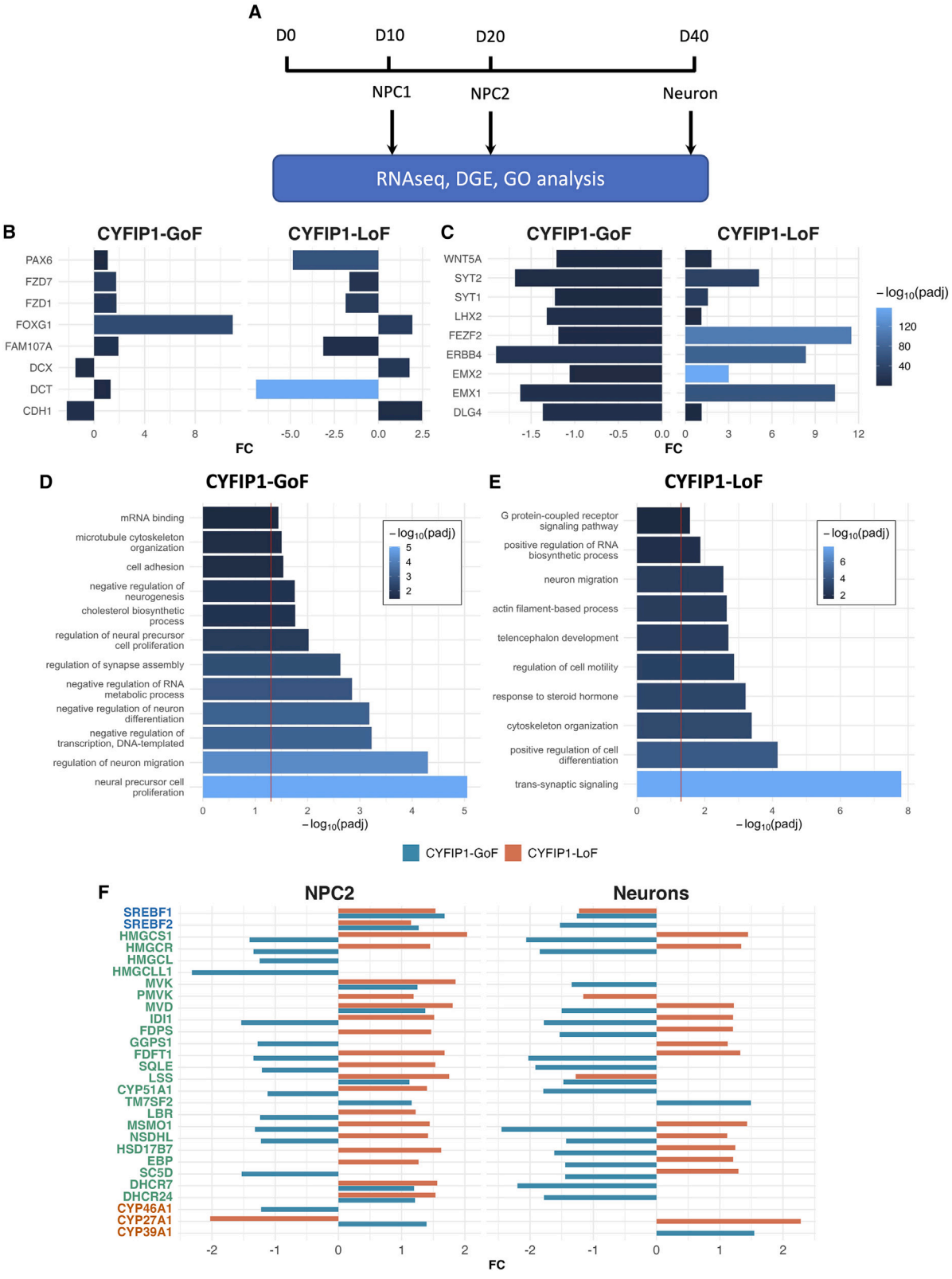

(legend on next page)

expression, mostly in contrasting directions, of genes involved in the cholesterol biosynthetic process (Figure 3F, Tables S2 and S3). Examples of these include *SREBF1* and *SREBF2*, the genes that encode the sterol regulatory element binding proteins 1 and 2 (SREBP1 and 2) required for fatty acid and cholesterol synthesis, and most of the genes for enzymes in the cholesterol biosynthesis cascade.

Convergent premature neuronal differentiation of 15q11.2del neural progenitors

CYFIP1 is one of the four genes in the 15q11.2 locus (*CYFIP1*, *NIPA1*, *NIPA2*, and *TUBGCP5*). To directly compare the cellular and molecular event consequent of CYFIP1-LoF and 15q11.2del, we derived iPSCs from two individuals carrying 15q11.2 deletions (referred to as EA8 and EA62, respectively) and control iPSCs from two unaffected controls (CTRL-iPSC). Following the same cortical differentiation paradigm, we observed evident reduction of CYFIP1 protein level in both NPCs and neurons derived from iPSCs of the two deletion carriers (two clones each) compared to respective control cell states (Figures S5A and S5B). Interestingly, NIPA2 expression was only detected in NPCs and not in neurons of either the control iPSC or 15q11.2del iPSC derivatives. 15q11.2del NPCs had a lower level of NIPA2 compared to the controls (Figures S5A and S5B). TUBGCP5 on the other hand was detected in both NPC and neuronal samples, and the expression level was not affected by 15q11.2 deletion (Figures S5A and S5B). We were not able to detect NIPA1 protein in any of the samples tested.

Similar to the observations made in CYFIP1-LoF cultures, 15q11.2del iPSC-derived cultures contained fewer $PAX6^+$ and $Ki67^+$ cells and more $P27^{kip1+}$ cells than the control cultures at d35 (Figures 4A–4C), indicating the presence of fewer dividing cells at this stage. We also observed a tendency of increased $TBR1^+$ and $CTIP2^+$ neurons in the two 15q11.2del iPSC cultures, although statistical significance was not reached for both lines at d30 (Figures 4D and 4E). Despite the line variations in temporal kinetics, these data nonetheless indicate that 15q11.2 deletion leads to premature neurogenesis, as observed in CYFIP1-LoF.

To gain further insights into the cellular and molecular changes caused by 15q11.2 deletion and investigate how these changes relate to loss of CYFIP1 alone, we carried out RNA-seq on d20 NPCs and d40 neurons derived from EA8 and EA62 iPSCs and a control iPSC line (Figure S5C). This experiment revealed around 2-fold reduction of *CYFIP1*, *NIPA1*, *NIPA2*, and *TUBGCP5* transcripts in samples from both deletion carriers (Figure S5D, Tables S6 and S7), reflecting the effect of the 15q11.2del and proving the reliability of our transcriptomic approach. Consistent with findings in the CYFIP1-LoF neural samples, GO analysis showed a significant dysregulation of biological processes related to sterol and cholesterol biosynthetic and metabolic process in both 15q11.2del iPSC lines (Figures 4F and 4G), with the master transcription factors *SREBF1* and *SREBF2* already upregulated at the progenitor stage and most of the enzyme-coding genes involved in cholesterol biosynthesis upregulated at the neuronal stage (Figure S5E; Tables S6 and S7). Moreover, cell proliferation and synaptic signaling were among the other significantly altered biological processes in samples from the two 15q11.2del carriers and both time points analyzed (Figures 4F and 4G, Tables S8 and S9).

Together, our findings demonstrate that 15q11.2 deletion results in phenotypic and transcriptomic alterations analogous to those caused by loss of CYFIP1 alone, highlighting a causal role for CYFIP1 in the pathological manifestations associated with 15q11.2 CNVs. Crucially, our transcriptomic analysis of both CYFIP1-manipulated and 15q11.2del neural cells revealed sterol biosynthesis as a CYFIP1-dependent function.

15q11.2del, CYFIP1-LoF, and CYFIP1-GoF cells display contrasting profile changes of 24S,25-epoxycholesterol

In light of the dysregulated cholesterol biosynthesis and metabolism revealed by the transcriptomics analysis, we performed a metabolic profiling of d20, d30, and d40 cortical cultures of all genotypes by liquid chromatography-mass spectrometry with multistage fragmentation ($LC\text{-}MS^n$). Consistently being detected in these samples were cholesterol precursors desmosterol and 8(9)-dehydrocholesterol, cholesterol itself, an immediate cholesterol metabolite 24S-hydroxycholeterol (24S-HC), and 24S,25-epoxycholesterol (24S,25-EC), an oxysterol generated in the shunt pathway during cholesterol biosynthesis and from desmosterol via oxidation by CYP46A1. Compared to the isogenic controls, CYFIP1-GoF cells had significantly lower levels of 24S,25-EC at all corresponding differentiation stages (Figure 5A). In contrast, CYFIP1-LoF samples showed an increased level of 24S,25-EC at d20 and d30 compared to the isogenic controls, while a significant increase of 24S,25-EC was observed at all time points for EA62 and at d20 for EA8 15q11.2del neural cells. An increase or decrease of desmosterol, cholesterol, and 24S-HC was observed in some CYFIP1-manipulated and 15q11.2del iPSC samples, although a consistent pattern of change was not observed for these sterol molecules (Figure S6).

24S,25-EC promotes neurogenesis and restores neuronal differentiation of CYFIP1- GoF cortical progenitors

24S,25-EC has been shown capable of promoting dopaminergic neuronal differentiation in hESC cultures and in the mouse

Figure 3. Genome-wide transcriptomic analysis of CYFIP1-GoF and CYFIP-LoF neural cells

(A) Schematic illustration of the RNA-seq experimental flow.

(B and C) Bar graphs showing examples of DEGs related to neural progenitors and neuronal differentiation at NPC2 (B) and neuronal stage (C), respectively. Bar height represents fold change, and the shade of color represents the FDR adjusted p value.

(D and E) Gene ontologies (GOs) enriched in the DEG datasets associated with CYFIP1-GoF (D) and CYFIP1-LoF (E), compared to the respective control samples for all developmental stages analyzed. Bar height represents the −log10 of the Benjamini-Hochberg adjusted p value, red line shows the threshold of significance (i.e., padj < 0.05).

(F) Bar graphs showing DEGs involved in cholesterol biosynthesis (green) and metabolism (red) and the master transcription factors for fatty acid and cholesterol biosynthesis (blue) at NPC2 and neuronal stages.

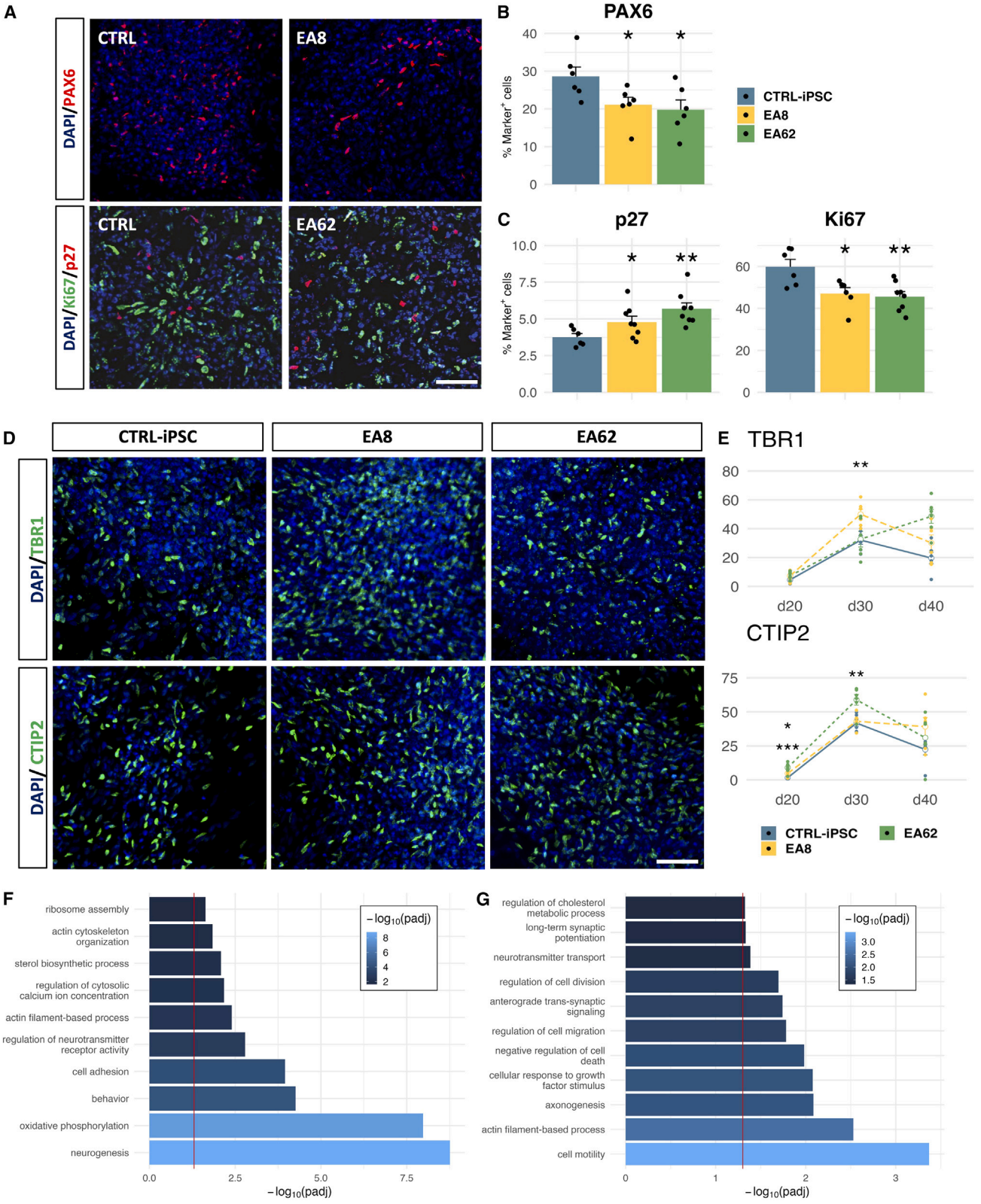

(legend on next page)

brain.[31–33] Due to its increased levels in 15q11.2del and CYFIP1-LoF samples and its concurrent decrease in CYFIP1-GoF cells, we tested the hypothesis that 24S,25-EC can promote cortical neuronal differentiation, which contributes to the premature neurogenesis of 15q11.2del and CYFIP1-LoF NPCs. H7 hPSC-derived cortical cultures were exposed to physiological concentrations of 24S,25-EC for 10 days during d15–25 and d20–30, respectively,[34–36] followed by immunostaining for TBR1, CTIP2, and NeuN (Figures 5B–5D). We observed a dose-dependent increase of CTIP2$^+$ neurons in cultures treated with 0.5–2 μM 24S,25-EC either from d15 or d20 (Figures 5C, 5D, S7A, and S7B). 24S,25-EC exposure also elicited an increase of TBR1$^+$ and NeuN$^+$ neurons in both experimental settings, although statistical significance was only reached under the d15–25 condition. TBR1$^+$ neurons are produced slightly earlier than CTIP2$^+$ cells in hPSC-derived cortical cultures, which may explain the diminishing effect of late 24S,25-EC treatment on TBR1$^+$ cells. Moreover, the neuronal promoting effect of 24S,25-EC was also observed in cortical neural cultures derived from the iCas9 hESC line (Figures S7C and S7D).

We next performed a cumulative EdU incorporation assay to investigate whether 24S,25-EC enhances neuronal differentiation by regulating cell cycle kinetics of the responding cells. D20 H7 cortical cultures were exposed to 24S,25-EC or ethanol control from 2 to 48 h followed by EdU staining. The cell-cycle (Tc) and S-phase (Ts) length were then calculated using the Nowakowski equation.[37] 24S,25-EC treatment did not affect the Tc but resulted in a dose-dependent decrease in Ts compared to ethanol controls (Figures 5E–5G). Consistent with this finding, we observed a reduction of Ki67$^+$ and phospho-histone H3$^+$ (PH3$^+$) cells after 4 days of 24S,25-EC treatment to d20 progenitors, indicating a decrease of total cycling cells (Figures S7E and S7F).

The neurogenic activity of 24S,25-EC observed above prompted us to ask whether this oxysterol can ameliorate reduced neuronal production of CYFIP1-GoF progenitors. We found that 0.5 μM 24S,25-EC treatment of CYFIP1-GoF culture during d15–25 was able to restore the number of TBR1$^+$ and CTIP2$^+$ neurons to the baseline H7 control levels indicated by the dashed lines (Figure 5H). Higher doses of 24S,25-EC resulted in a further increase of neuronal numbers in CYFIP1-GoF cultures, providing additional support for the dose dependence on 24S,25-EC. Since 24S,25-EC level was reduced in CYFIP1-GoF cultures, the increase of neuronal numbers in 24S,25-EC-treated CYFIP1-GoF cultures presents a rescue of the neurogenesis defect in these cells and provides evidence for the role of 24S,25-EC dysregulation in the CYFIP1-GoF phenotype. Interestingly, the fold changes of neuronal numbers relative to vehicle control in responding to increasing 24S,25-EC concentration were statistically comparable between the CYFIP1-GoF and H7 isogenic control cultures despite the lower absolute neuron numbers in CYFIP1-GoF cultures in the basal condition or when treated with 24S,25-EC of the same doses (Figures 5H and S7G). This observation indicates comparable responsiveness of CYFIP1-GoF cells to 24S,25-EC compared to H7 isogenic controls.

LXR signaling mediates oxysterol regulation of neurogenesis in hPSC-derived cortical progenitors

A number of oxysterols, including 24S,25-EC, have been identified as endogenous ligands of LXR,[38,39] raising the question of whether LXR signaling plays a role in CYFIP1 regulation of neurogenesis. LXRβ is the dominant isoform expressed in the brain and functions via forming obligatory heterodimer with retinoid X receptor (RXR).[40] We therefore analyzed the RNA-seq dataset further for differential expression of LXRβ, RXR, and their target genes in 15q11.2del, CYFIP1-LoF, and CYFIP1-GoF NPCs and neurons compared to their respective controls.[41,42] We found that while no significant changes were detected in the transcript levels of LXRβ and RXR themselves, many of the LXRβ and RXR target genes were among the DEGs of CYFIP1-GoF, CYFIP1-LoF, and the two 15q11.2del lines at both NPC and neuronal stages. Examples include master transcription factor for sterol biosynthesis (SREBF1), genes involved in neural progenitor proliferation and differentiation (ID1 and 2, HEY1, SMAD3 and 5), and G1 cell cycle phase progression (CDK4, Tables S2, S3, S6, and S7). Fisher exact test confirmed significant enrichment of LXRβ target DEGs against the total non-LXR target DEGs in CYFIP1-GoF NPCs, CYFIP1-LoF NPCs and neurons, and EA8 iPSC NPCs, while RXR targets were also significantly enriched in CYFIP1-GoF NPCs and EA8 iPSC NPCs and neurons (Figure 6A). Thus, the transcriptomics data indicate altered LXR signaling in neural cells with 15q11.2del, CYFIP1-LoF, and CYFIP1-GoF.

In order to provide direct evidence that LXR signaling mediates oxysterol regulation of neuronal differentiation, we generated a loss-of-function LXRβ (NR1H2) line via CRISPR-Cas9 genome editing in iCas9 hESCs (referred to as LXRβ$^{-/-}$) and examined the response of LXRβ$^{-/-}$ NPCs to 24S,25-EC using the same experimental paradigm as described above (Figures 5 and S8). In contrast to that observed in H7 and iCas9 cultures treated with 24S,25-EC (Figures 5C, 5D, and S7), no differences in the number of TBR1$^+$, CTIP2$^+$, and NeuN$^+$ neurons were detected between the vehicle control and 24S,25-EC-treated

Figure 4. 15q11.2del iPSCs display a similar neurogenesis phenotype to that of CYFIP1-LoF

(A) Two clones each of EA8 and EA62 15q11.2del lines and two control iPSC lines were differentiated toward cortical fate, and immunostaining was performed at d35 cultures for PAX6 (red), Ki67 (green), and p27^{kip1} (red).

(B and C) Quantification data for the proportion of PAX6$^+$, Ki67$^+$, and p27^{kip1+} cells.

(D) Immunostaining performed at d30 for deep-layer cortical neuronal markers TBR1 and CTIP2 (green).

(E) Quantification data for the proportion of TBR1$^+$ and CTIP2$^+$ cells at d20, d30, and d40.

(F and G) Gene ontologies (GOs) enriched in the DEG datasets associated with EA8 (F) and EA62 (G) compared to the control iPSC samples. Bar height represents the −log10 padj value, and red line shows the threshold of significance (i.e., padi < 0.05). Each dot in (B), (C), and (E) represents a biological replicate. Data represent mean ± SEM of six biological replicates with the lines used detailed in Table S10. Groups were compared by Student's t test between the control and 15q11.2del cells per time point (*p < 0.05, **p < 0.01). Nuclei were counterstained with DAPI (blue). Scale bars: 50 μm.

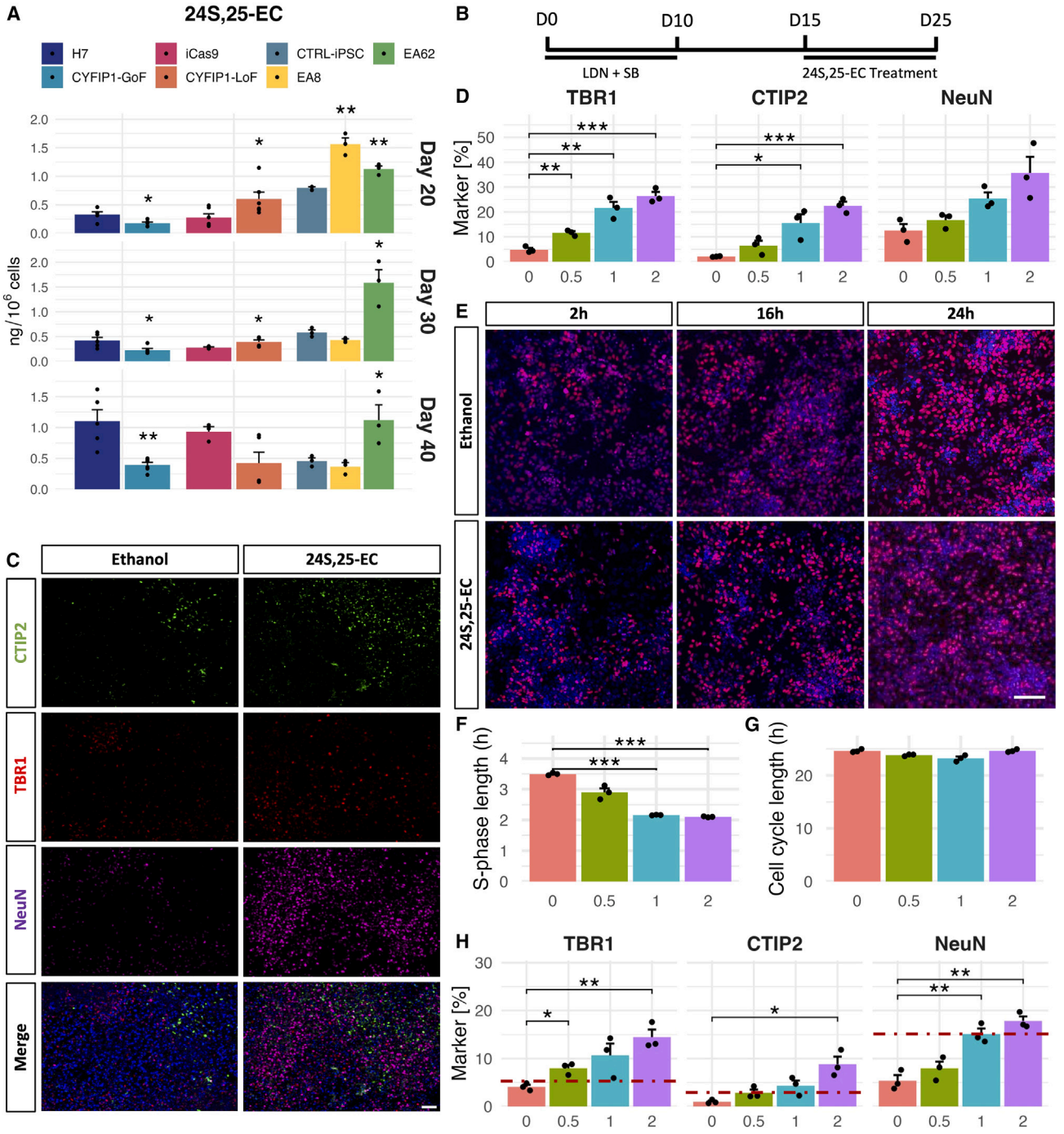

Figure 5. 24S,25-EC promotes neuronal differentiation of hESC-derived cortical NPCs

(A) Bar graph showing the levels of 24S,25-EC produced by CYFIP1-GoF, CYFIP1-LoF, EA8, and EA62 15q11.2del iPSCs and respective control PSC-derived neural cells at d20, d30, and d40. n = 5 or 6 as indicated in Table S10.

(B) Schematic illustration showing 24S,25-EC treatment time windows.

(C) Representative images of immunostaining for TBR1, CTIP2, and NeuN at d25 H7 cultures treated with ethanol vehicle control and 24S,25-EC between d15 and d25.

(D) Quantification of the immunocytochemical analysis represented in (C), n = 3.

(E–G) Cumulative EdU incorporation assay of H7 cortical progenitor cultures treated with vehicle and increasing doses of 24S,25-EC from d15. Representative images of EdU$^+$ cells (E). Length of S-phase (F) and total cell cycle (G) determined by Nowakowski equation for all conditions, n = 3.

(legend continued on next page)

LXRβ$^{-/-}$ cultures (Figures 6B and 6C). This finding demonstrates that LXRβ is required for 24S,25-EC regulation of neurogenesis.

LXRβ knockout attenuates premature neuronal differentiation of CYFIP1-deficient cortical progenitors

24S,25-EC levels were increased in CYFIP1-LoF and 15q11.2del cells, accompanied by apparent over-activation of LXR signaling in these cells as suggested by the transcriptomics analysis. These findings point to the hypothesis that dysregulated LXR signaling underlies the premature neuronal differentiation, and its blockade would rescue or partially rescue this deficit. To this end, we also genetically deleted LXRβ in a CYFIP1-LoF line (CYFIP1$^{-/-}$LXRβ$^{-/-}$) and examined the consequence of CYFIP1/LXRβ compound deletion on neuronal production in comparison with the isogenic trios of CYFIP1$^{-/-}$, LXRβ$^{-/-}$, and iCas9 hESCs. We found that LXRβ single knockout did not affect the number of TBR1^{+}, CTIP2^{+}, and NeuN^{+} neurons compared to its isogenic iCas9 control (Figures 6D and 6E). As expected, neuronal production was increased in CYFIP1-LoF cultures at d30. However, the double-knockout cultures contained a comparable number of neurons to that of the iCas9 cultures (Figures 6D and 6E), indicating that ablation of LXRβ in CYFIP1$^{-/-}$ neural progenitors attenuated the premature neuronal differentiation due to CYFIP1 deficiency. This result demonstrates that LXR signaling serves as a mechanism underlying the aberrant neurogenesis in CYFIP1 and 15q11.2del cortical cultures.

DISCUSSION

The notion that changes in temporal dynamics of developmental processes underlie neurodevelopmental disorders is gaining momentum,[43–46] but precise molecular mechanisms have remained largely unknown. The autism risk gene CYFIP1 has been primarily studied for its role in synaptic plasticity. Here, we report an early developmental role for CYFIP1 and identify CYFIP1 control of cholesterol biosynthesis as a regulatory axis playing an important role in neurogenesis. Our findings suggest that dysregulation of oxysterol-regulated LXR signaling consequent of 15q11.2CNVs may contribute to the pathogenesis of associated neurological disorders.

CYFIP1, a regulator of neurogenesis and causal risk gene in 15q11.2 loci

Being part of the WAVE regulatory complex and binding partner of FMRP, respectively, CYFIP1 plays an important role in actin cytoskeleton formation and protein translation. Accordingly, CYFIP1 functions have been reported in neural progenitor migration,[20] brain structure,[18,19] dendritic morphology,[13,14] synaptic activity, and associated behaviors.[12,15,47] Recent mouse genetic studies also revealed a role for Cyfip1 in adult neurogenesis, although opposite effects were reported.[16,17] The underlying molecular mechanisms by which Cyfip1 affects adult neural stem cells in these mouse models remain unknown, however. The current study uncovered a requirement for CYFIP1 in neurogenesis early in the embryonic stages, a cellular function in line with its expression during human cortical development. Both CYFIP1 deficiency and its elevated expression led to disturbed neurogenesis, suggesting that a tight control of CYFIP1 level is crucial for coordinated neural progenitor proliferation and terminal differentiation. Inappropriate neuronal numbers and/or birth time of a defined subtype may result in errors in their final destinations and mismatched neuronal interconnections in the brain, which may contribute to the mirror phenotypes in MRI studies of white matter microstructure and the network dysfunction present in patients with neurodevelopmental disorders attributed to CNVs at the 15q11.2 locus.[48]

CYFIP1 is generally considered as the major risk gene within the 15q11.2 locus that impacts adverse neurological outcomes,[35,49] but direct evidence for this has been lacking. Using the same neuronal differentiation paradigm, we show that NPCs derived from 15q11.2del iPSCs present a closely analogous phenotype to hESC-derived NPCs deficient in CYFIP1 alone. Consistent with the experimental findings, genome-wide transcriptomic analysis revealed significant dysregulation of transcripts related to neurogenesis from both CYFIP1-modified hESC- and 15q11.2del iPSC-neural derivatives and, crucially, a high degree of overlap in the biological processes (GO terms), despite the variations between independent carrier iPSC lines and that CYFIP1-GoF and CYFIP1-LoF cells were derived in different parental lines. Therefore, our work provides a direct demonstration for CYFIP1 as the likely causal risk factor of 15q11.2 deletion effects on neurogenesis.

Oxysterol regulation of cortical neurogenesis and implications in pathogenesis of neurodevelopmental disorders

The work presented here identified a pro-neuron differentiation activity of 24S,25-EC in human cortical progenitors. 24S,25-EC has been shown to be abundantly produced in the developing mouse cortex,[34] while Wong et al. also detected this oxysterol in primary cultured human fetal cortical neurons.[50] We found in this study that 24S,25-EC is already produced by d20 human NPCs at comparable levels to that of d30–d40 neuronal cultures. These findings together support a physiological role of 24S,25-EC in regulating cortical NPC differentiation in the fetal brain, as it has been shown previously in the developing ventral midbrain.[31–33] 24S-HC is another LXR binding oxysterol consistently being detected in the current study. In contrast to 24S,25-EC, 24S-HC is present at a higher level in the adult brain than the developing brain and is believed to be primarily synthesized in neurons.[34] We didn't observe a consistent change in 24S-HC levels in our CYFIP1-manipulated and 15q11.2del samples. Nevertheless, given its relevance to brain diseases,[51] future investigations into a potential activity of this oxysterol in

(H) Quantification of TBR1^{+}, CTIP2^{+}, and NeuN^{+} in d25 CYFIP1-GoF cultures after 10 days of exposure to increasing dose of 24S,25-EC or ethanol control. The red dashed line indicates the baseline (untreated) level in the isogenic control line, n = 3. Data shown are mean ± SEM of the number of biological replicates indicated in specific panels. Groups were compared by Student's t test between the indicated genotype and respective control per time point in (A) and one-way ANOVA followed by Tukey's correction for (D) and (F)–(H) (*p < 0.05; **p < 0.01; ***p < 0.001). Nuclei were counterstained with DAPI (blue). Scale bars: 50 μm.

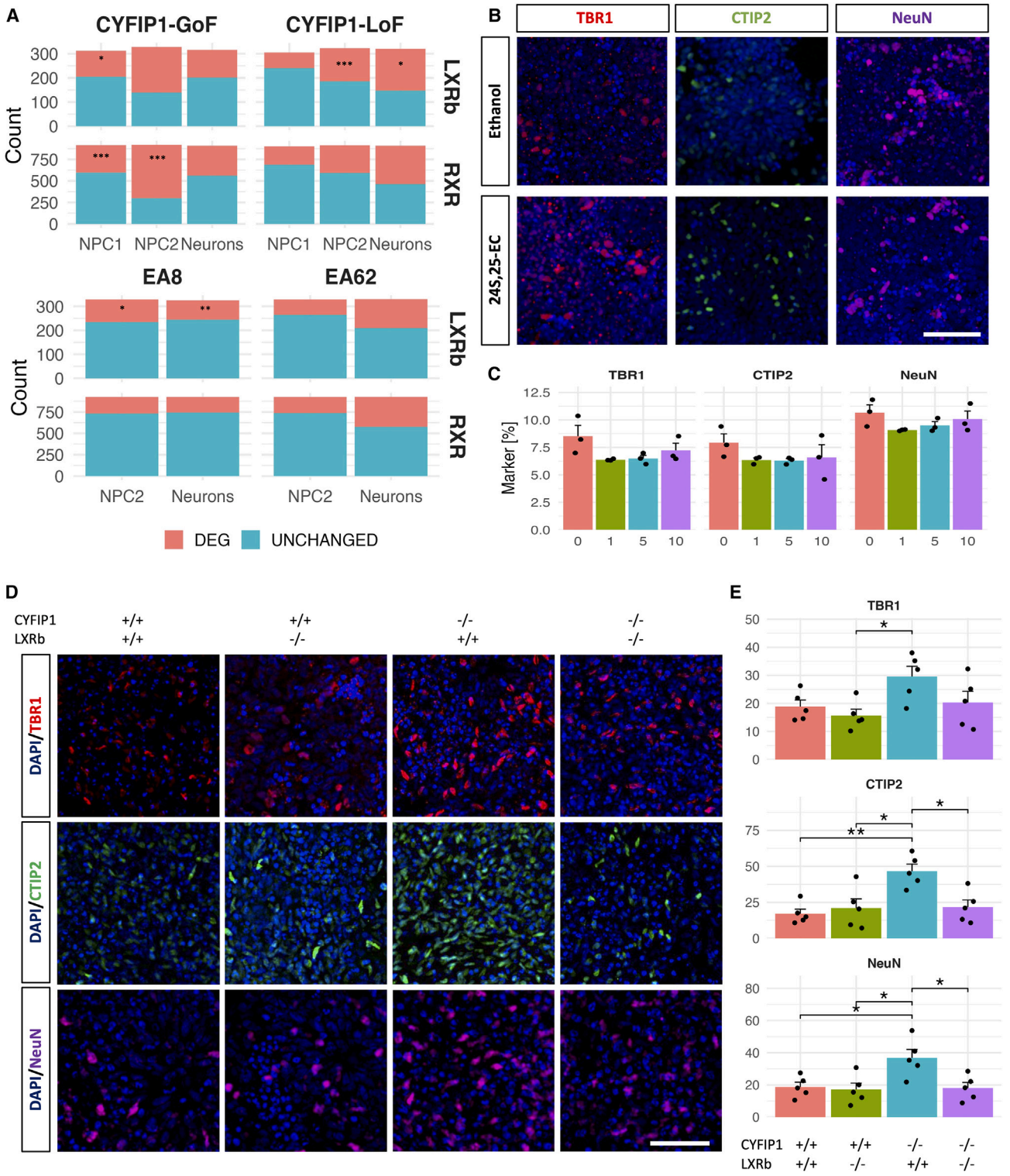

Figure 6. LXR signaling mediates oxysterol-regulated neurogenesis

(A) Bar graph showing the number of differentially expressed LXRβ and RXR target genes in CYFIP1-GoF, CYFIP1-LoF, and 15q11.2del NPCs and neurons. LXRβ and RXR targets were compared to non-target DEGs by one-sided Fisher's exact test (*$p < 0.05$; **$p < 0.01$; ***$p < 0.001$).

(B and C) 24S,25-EC treatment during d15–d25 failed to promote neuronal production of LXRβ-deficient NPCs.

(legend continued on next page)

neurogenesis either on its own or in cooperation with 24S,25-EC would be beneficial.

Does 24S,25-EC target NPCs promiscuously or defined progenitor subtypes? In the embryonic cortex, neurons are produced from both apical and basal progenitors, while apical progenitors also give rise to basal progenitors. The human brain generates more basal progenitors during development as a strategy to produce more neurons. Basal progenitors have a longer cell cycle (Tc) than apical progenitors, while the expanding (proliferating) neural progenitors, both apical and basal, shorten S-phase length (Ts) when they commit to neuronal production.[52] 24S,25-EC shortens the Ts of hESC-derived cortical progenitors without affecting Tc, suggesting it may promote the transition from expanding neural progenitors to neurogenic progenitors, regardless of they are apical or basal progenitors.

The discovery that 15q11.2del and CYFIP1 dosage change led to abnormal 24S,25-EC production points to a causal link between distorted sterol biosynthesis and autism and schizophrenia, while the ability of 24S,25-EC and genetic blockade of its downstream signaling (via LXRβ knockout; see discussion below) in restoring delayed and premature neuronal differentiation of CYFIP1-GoF and CYFIP1-LoF NPCs, respectively, implicates a potential role for distorted sterol biosynthesis in the pathogenesis of 15q11.2CNV-associated disorder. It would be interesting to investigate whether sterol dysregulation also plays a role in neurodevelopmental disorders associated with other risk genes/loci. Relevant to this hypothesis, changes in SREBP2 and CYP46A1 protein levels have been reported in several brain regions in a preclinical model of fragile X syndrome.[53]

A role for oxysterols in pathogenesis of neurodevelopmental disorder was also suggested by a recent study of mouse and hESC models of Smith-Lemli-Opitz syndrome (SLOS).[54] SLOS is caused by mutations in the cholesterol biosynthesis gene 7-dehydrocholesterol reductase (DHCR7) that converts 7-dehydrocholesterol (7-DHC) to cholesterol. SLOS patients present a host of neurodevelopmental abnormalities including small head size (microcephaly), severe developmental delay, and features of autism.[55] Loss of Dhcr7/DHCR7 alleles results in decreased proliferation and increased neurogenesis in the developing mouse cortex and hESC-derived cortical progenitors, caused by an accumulation of 7-DHC and 7-DHC-derived oxysterols.[54]

Several recent studies highlighted the potential for brain-derived oxysterols as biomarkers of neurodegenerative conditions such as Alzheimer's disease.[56] Unlike cholesterol, oxysterols readily traverse the blood-brain barrier from the brain to periphery and vice versa; thus plasma levels of brain-derived oxysterols reflect cholesterol biosynthesis and metabolism in the brain.[57] Altered oxysterol levels have been described in patients with several neurodegenerative disorders, including Alzheimer's disease, amyotrophic lateral sclerosis, Parkinson's disease, and Huntington's disease.[58–60] While investigation into sterol dysregulation in neuropsychiatric and neurodevelopmental disorders is in its infancy, changes of plasma 24S-HC are found in patients with schizophrenia,[61] ASD,[62] and bipolar disorders.[63]

Molecular mechanisms underlying CYFIP1 regulation of neurogenesis

Accelerated or delayed neurogenic differentiation, often exemplified by alterations of neural progenitor to neuron ratio during early neurogenesis, have been reported in multiple studies of human stem cell models carrying neurodevelopmental risk variants.[31,43–46,64] However, the molecular mechanisms responsible for the disrupted process remain largely unknown. By demonstrating the loss of pro-neuronal activity of 24S,25-EC and the rescue of premature neuronal differentiation of CYFIP1-LoF NPCs by genetic deletion of LXRβ, respectively, the work described here establishes LXR as the overriding signaling mechanism underlying the disturbed neurogenesis in CYFIP1-LoF. This finding is consistent with a previous report that 24S,25-EC is a potent endogenous ligand of LXR as well as being the most abundant LXR ligand over other oxysterols in the developing brain playing a role in midbrain dopaminergic neurogenesis *in vivo*.[31,33,34]

Several lines of evidence support a direct regulatory role of CYFIP1 in cholesterol biosynthesis. CYFIP1 is known to regulate protein translation via binding to mRNA targets as part of the protein complex with FMRP and eIF4E.[9,65] SREBP1 and SREBP2 are master transcription factors for genes regulating lipid homeostasis. SREBP1 regulates lipogenic genes, whereas SREBP2 preferentially activates genes of cholesterol biosynthesis and metabolism.[66,49] SREBP2 RNA has been shown recently as a direct target of CYFIP1 in the adult mouse cortical and hippocampus tissues via RNA immunoprecipitation sequencing (RIP-seq) against CYFIP1.[47] Moreover, SREBP2 was also identified as a high-confidence FMRP target in the brain, together with RNAs for two enzymes in the cholesterol synthesis pathway—HMGCS1 (hydroxymethylglutaryl-CoA synthase) and GGPS1 (geranylgeranyl diphosphate)[67,68]—while SREBP1 and 14 other genes in the cholesterol synthesis pathway are reported to bind to FMRP in HEK cells.[69] In line with the above, the majority of genes involved in cholesterol biosynthesis and metabolism are differentially expressed, mostly in opposite direction of change in CYFIP1-GoF and CYFIP1-LoF neural progenitors and neurons (Figure 3F), and the transcriptomic changes are in line with the alteration of 24S,25-EC in neural cells of respective genotypes (Figure 5A). Together, these findings provide a mechanistic link between CYFIP1 dosage change and alteration of neural sterol profile in 15q11.2del and CYFIP1-disrupted PSC neural derivatives.

In summary, this study revealed a role for CYFIP1 within the 15q11.2 CNV in human neurogenesis, which is mediated by the oxysterol-LXR signaling axis through alterations in cholesterol metabolism. This mechanistic insight opens fresh perspectives to approach neuropsychiatric and neurodevelopmental disorders. Given the potential of oxysterols as disease biomarkers and druggable targets, this study may shed light into

(D and E) Premature neuronal differentiation of CYFIP1-LoF NPC is reversed by compound deletion of LXRβ and CYFIP1. Data shown in (C) and (E) are mean ± SEM from three (C) and five (D) biological replicates per treatment or genotype. Groups were compared by one-way ANOVA followed by Tukey's correction (*$p < 0.05$; **$p < 0.01$; ***$p < 0.001$). Nuclei were counterstained with DAPI (blue). Scale bars: 50 μm.

the development of better diagnostic and therapeutic avenues in associated neurological disorders.

Limitations of the study

In this study, 15q11.2del iPSC-derived cortical progenitors showed the same direction of changes to that of CYFIP1-LoF in premature neuronal differentiation, differential expression of genes controlling cholesterol metabolism, and targets of LXR. However, the two 15q11.2del iPSC lines varied from each other in their differentiation tempo, which likely contributed to the fewer DEGs and overall weaker phenotype detected in 15q11.2del iPSCs. These observations reinforce the importance of generating CRISPR-corrected patient iPSC lines as isogenic controls in disease modeling. Additionally, the current work studies a single variant conferring risk to autism and schizophrenia, and further investigation of iPSC models carrying other disease risk genes is required to examine a potential convergent role for cholesterol metabolism and oxysterol-LXR signaling in the pathogenesis of neuropsychiatric and neurodevelopmental disorders.

STAR★METHODS

Detailed methods are provided in the online version of this paper and include the following:

- KEY RESOURCES TABLE
- RESOURCE AVAILABILITY
  - Lead contact
  - Materials availability
  - Data and code availability
- EXPERIMENTAL MODEL AND SUBJECT DETAILS
  - Generation of CYFIP1-GoF and CYFIP1-LoF PSC lines by transgene expression and CRISPR/Cas9 assisted genome editing
  - iPSC reprograming and quality control analysis
- METHOD DETAILS
  - Stem cell culture and differentiation
  - Immunocytochemistry
  - EdU labeling and detection
  - Flow cytometry
  - Quantitative PCR
  - RNA extraction and bulk RNA sequencing
  - Analysis of RNA sequencing data
  - Western Blot
  - Sterol extraction, derivatization and LC-MS
- QUANTIFICATION AND STATISTICAL ANALYSES

SUPPLEMENTAL INFORMATION

Supplemental information can be found online at https://doi.org/10.1016/j.celrep.2024.113946.

ACKNOWLEDGMENTS

We thank Drs. William Griffiths and Yuqin Wang for the mass spectrometry performed in their laboratories and for providing expert advice on oxysterol-related neuronal assays. We thank Drs. Stefanie Linden, Faraz Ali, Kali Barawi, Jacqueline Smith, and Alister Baird and support from Welsh National Center for Mental Health for providing 15q11.2del biopsies, and we also thank Dr. Craig Joyce for iPSC reprograming. RNA sequencing analysis was performed using the computational facilities of the Advanced Research Computing@Cardiff (ARCCA) Division, Cardiff University. This work was supported by a Wellcome Trust Strategic Award (100202/Z/12/Z) to M.J.O., J.H., D.E.J.L., M.L., and other co-PIs and funding from the Medical Research Council (MRC, grant no. MR/R022429/1 to M.L.). The mass spectrometry work and equipment was funded by Swansea University, the Biotechnology and Biological Sciences Research Council (BBSRC, grant no. BB/S019588/1), and the Wellcome Trust Strategic Award (100202/Z/12/Z) through M.L. E.S. is funded by a BBSRC SWBio PhD studentship. For the purpose of open access, the author has applied a Creative Commons Attribution (CC BY) license to any author-accepted manuscript version arising from this submission.

AUTHOR CONTRIBUTIONS

M.L., C.T., and D.C.D.L.F. conceived the study and designed the experiments. D.C.D.L.F. and C.T. carried out and analyzed the hESC and hiPSC experiments. D.C.D.L.F. performed RNA-seq data analysis with support from A.P. and R.A. E.S. performed the sterol profiling and analyzed the data. D.E.J.L., J.H., and M.J.O. provided 15q11.2del carrier samples and contributed to general discussions throughout the work. M.L., C.T., and D.C.D.L.F. wrote the paper. All authors edited and approved the paper.

DECLARATION OF INTERESTS

The authors declare no competing financial interests.

Received: June 23, 2023
Revised: December 22, 2023
Accepted: February 26, 2024

REFERENCES

1. Gejman, P.V., Sanders, A.R., and Kendler, K.S. (2011). Genetics of schizophrenia: new findings and challenges. Annu. Rev. Genomics Hum. Genet. *12*, 121–144. https://doi.org/10.1146/annurev-genom-082410-101459.
2. International Schizophrenia Consortium (2008). Rare chromosomal deletions and duplications increase risk of schizophrenia. Nature *455*, 237–241. https://doi.org/10.1038/nature07239.
3. Kirov, G., Grozeva, D., Norton, N., Ivanov, D., Mantripragada, K.K., Holmans, P., International Schizophrenia Consortium; Wellcome Trust Case Control Consortium; Craddock, N., Owen, M.J., et al. (2009). Support for the involvement of large copy number variants in the pathogenesis of schizophrenia. Hum. Mol. Genet. *18*, 1497–1503. https://doi.org/10.1093/hmg/ddp043.
4. Kirov, G., Rees, E., Walters, J.T.R., Escott-Price, V., Georgieva, L., Richards, A.L., Chambert, K.D., Davies, G., Legge, S.E., Moran, J.L., et al. (2014). The penetrance of copy number variations for schizophrenia and developmental delay. Biol. Psychiatry *75*, 378–385. https://doi.org/10.1016/j.biopsych.2013.07.022.
5. Rees, E., Walters, J.T.R., Georgieva, L., Isles, A.R., Chambert, K.D., Richards, A.L., Mahoney-Davies, G., Legge, S.E., Moran, J.L., McCarroll, S.A., et al. (2014). Analysis of copy number variations at 15 schizophrenia-associated loci. Br. J. Psychiatry *204*, 108–114. https://doi.org/10.1192/bjp.bp.113.131052.
6. Stefansson, H., Meyer-Lindenberg, A., Steinberg, S., Magnusdottir, B., Morgen, K., Arnarsdottir, S., Bjornsdottir, G., Walters, G.B., Jonsdottir, G.A., Doyle, O.M., et al. (2014). CNVs conferring risk of autism or schizophrenia affect cognition in controls. Nature *505*, 361–366. https://doi.org/10.1038/nature12818.
7. Picinelli, C., Lintas, C., Piras, I.S., Gabriele, S., Sacco, R., Brogna, C., and Persico, A.M. (2016). Recurrent 15q11.2 BP1-BP2 microdeletions and microduplications in the etiology of neurodevelopmental disorders. Am. J.

Med. Genet. B Neuropsychiatr. Genet. *171*, 1088–1098. https://doi.org/10.1002/ajmg.b.32480.

8. Chai, J.H., Locke, D.P., Greally, J.M., Knoll, J.H.M., Ohta, T., Dunai, J., Yavor, A., Eichler, E.E., and Nicholls, R.D. (2003). Identification of four highly conserved genes between breakpoint hotspots BP1 and BP2 of the Prader-Willi/Angelman syndromes deletion region that have undergone evolutionary transposition mediated by flanking duplicons. Am. J. Hum. Genet. *73*, 898–925. https://doi.org/10.1086/378816.
9. Napoli, I., Mercaldo, V., Boyl, P.P., Eleuteri, B., Zalfa, F., De Rubeis, S., Di Marino, D., Mohr, E., Massimi, M., Falconi, M., et al. (2008). The fragile X syndrome protein represses activity-dependent translation through CYFIP1, a new 4E-BP. Cell *134*, 1042–1054. https://doi.org/10.1016/j.cell.2008.07.031.
10. Schenck, A., Bardoni, B., Moro, A., Bagni, C., and Mandel, J.L. (2001). A highly conserved protein family interacting with the fragile X mental retardation protein (FMRP) and displaying selective interactions with FMRP-related proteins FXR1P and FXR2P. Proc. Natl. Acad. Sci. USA *98*, 8844–8849. https://doi.org/10.1073/pnas.151231598.
11. Chen, Z., Borek, D., Padrick, S.B., Gomez, T.S., Metlagel, Z., Ismail, A.M., Umetani, J., Billadeau, D.D., Otwinowski, Z., and Rosen, M.K. (2010). Structure and control of the actin regulatory WAVE complex. Nature *468*, 533–538. https://doi.org/10.1038/nature09623.
12. Davenport, E.C., Szulc, B.R., Drew, J., Taylor, J., Morgan, T., Higgs, N.F., López-Doménech, G., and Kittler, J.T. (2019). Autism and Schizophrenia-Associated CYFIP1 Regulates the Balance of Synaptic Excitation and Inhibition. Cell Rep. *26*, 2037–2051.e6. https://doi.org/10.1016/j.celrep.2019.01.092.
13. Oguro-Ando, A., Rosensweig, C., Herman, E., Nishimura, Y., Werling, D., Bill, B.R., Berg, J.M., Gao, F., Coppola, G., Abrahams, B.S., and Geschwind, D.H. (2015). Increased CYFIP1 dosage alters cellular and dendritic morphology and dysregulates mTOR. Mol. Psychiatry *20*, 1069–1078. https://doi.org/10.1038/mp.2014.124.
14. Pathania, M., Davenport, E.C., Muir, J., Sheehan, D.F., López-Doménech, G., and Kittler, J.T. (2014). The autism and schizophrenia associated gene CYFIP1 is critical for the maintenance of dendritic complexity and the stabilization of mature spines. Transl. Psychiatry *4*, e374. https://doi.org/10.1038/tp.2014.16.
15. Sahasrabudhe, A., Begum, F., Guevara, C.A., Morrison, C., Hsiao, K., Kezunovic, N., Bozdagi-Gunal, O., and Benson, D.L. (2020). Cyfip1 regulates syngap1 at hippocampal synapses. Front. Synaptic Neurosci. *12*, 581714. https://doi.org/10.3389/fnsyn.2020.581714.
16. Haan, N., Westacott, L.J., Carter, J., Owen, M.J., Gray, W.P., Hall, J., and Wilkinson, L.S. (2021). Haploinsufficiency of the schizophrenia and autism risk gene Cyfip1 causes abnormal postnatal hippocampal neurogenesis through microglial and Arp2/3 mediated actin dependent mechanisms. Transl. Psychiatry *11*, 313. https://doi.org/10.1038/s41398-021-01415-6.
17. Habela, C.W., Yoon, K.-J., Kim, N.-S., Taga, A., Bell, K., Bergles, D.E., Maragakis, N.J., Ming, G.-L., and Song, H. (2020). Persistent cyfip1 expression is required to maintain the adult subventricular zone neurogenic niche. J. Neurosci. *40*, 2015–2024. https://doi.org/10.1523/JNEUROSCI.2249-19.2020.
18. Domínguez-Iturza, N., Lo, A.C., Shah, D., Armendáriz, M., Vannelli, A., Mercaldo, V., Trusel, M., Li, K.W., Gastaldo, D., Santos, A.R., et al. (2019). The autism- and schizophrenia-associated protein CYFIP1 regulates bilateral brain connectivity and behaviour. Nat. Commun. *10*, 3454. https://doi.org/10.1038/s41467-019-11203-y.
19. Silva, A.I., Haddon, J.E., Ahmed Syed, Y., Trent, S., Lin, T.-C.E., Patel, Y., Carter, J., Haan, N., Honey, R.C., Humby, T., et al. (2019). Cyfip1 haploinsufficient rats show white matter changes, myelin thinning, abnormal oligodendrocytes and behavioural inflexibility. Nat. Commun. *10*, 3455. https://doi.org/10.1038/s41467-019-11119-7.
20. Yoon, K.-J., Nguyen, H.N., Ursini, G., Zhang, F., Kim, N.-S., Wen, Z., Makri, G., Nauen, D., Shin, J.H., Park, Y., et al. (2014). Modeling a genetic risk for schizophrenia in iPSCs and mice reveals neural stem cell deficits associated with adherens junctions and polarity. Cell Stem Cell *15*, 79–91. https://doi.org/10.1016/j.stem.2014.05.003.
21. González, F., Zhu, Z., Shi, Z.-D., Lelli, K., Verma, N., Li, Q.V., and Huangfu, D. (2014). An iCRISPR platform for rapid, multiplexable, and inducible genome editing in human pluripotent stem cells. Cell Stem Cell *15*, 215–226. https://doi.org/10.1016/j.stem.2014.05.018.
22. Nowakowski, T.J., Bhaduri, A., Pollen, A.A., Alvarado, B., Mostajo-Radji, M.A., Di Lullo, E., Haeussler, M., Sandoval-Espinosa, C., Liu, S.J., Velmeshev, D., et al. (2017). Spatiotemporal gene expression trajectories reveal developmental hierarchies of the human cortex. Science *358*, 1318–1323. https://doi.org/10.1126/science.aap8809.
23. Nguyen, L., Besson, A., Heng, J.I.-T., Schuurmans, C., Teboul, L., Parras, C., Philpott, A., Roberts, J.M., and Guillemot, F. (2006). p27kip1 independently promotes neuronal differentiation and migration in the cerebral cortex. Genes Dev. *20*, 1511–1524. https://doi.org/10.1101/gad.377106.
24. Bishop, K.M., Garel, S., Nakagawa, Y., Rubenstein, J.L.R., and O'Leary, D.D.M. (2003). Emx1 and Emx2 cooperate to regulate cortical size, lamination, neuronal differentiation, development of cortical efferents, and thalamocortical pathfinding. J. Comp. Neurol. *457*, 345–360. https://doi.org/10.1002/cne.10549.
25. Harrison, S.J., Nishinakamura, R., Jones, K.R., and Monaghan, A.P. (2012). Sall1 regulates cortical neurogenesis and laminar fate specification in mice: implications for neural abnormalities in Townes-Brocks syndrome. Dis. Model. Mech. *5*, 351–365. https://doi.org/10.1242/dmm.002873.
26. Zhou, X., Zhong, S., Peng, H., Liu, J., Ding, W., Sun, L., Ma, Q., Liu, Z., Chen, R., Wu, Q., and Wang, X. (2020). Cellular and molecular properties of neural progenitors in the developing mammalian hypothalamus. Nat. Commun. *11*, 4063. https://doi.org/10.1038/s41467-020-17890-2.
27. Jiao, Z., Zhang, Z.G., Hornyak, T.J., Hozeska, A., Zhang, R.L., Wang, Y., Wang, L., Roberts, C., Strickland, F.M., and Chopp, M. (2006). Dopachrome tautomerase (Dct) regulates neural progenitor cell proliferation. Dev. Biol. *296*, 396–408. https://doi.org/10.1016/j.ydbio.2006.06.006.
28. Greif, K.F., Asabere, N., Lutz, G.J., and Gallo, G. (2013). Synaptotagmin-1 promotes the formation of axonal filopodia and branches along the developing axons of forebrain neurons. Dev. Neurobiol. *73*, 27–44. https://doi.org/10.1002/dneu.22033.
29. Bonafina, A., Fontanet, P.A., Paratcha, G., and Ledda, F. (2018). GDNF/GFRα1 Complex Abrogates Self-Renewing Activity of Cortical Neural Precursors Inducing Their Differentiation. Stem Cell Rep. *10*, 1000–1015. https://doi.org/10.1016/j.stemcr.2018.01.019.
30. Gupta, S.J., Churchward, M.A., Todd, K.G., and Winship, I.R. (2023). Pleiotrophin signals through ALK receptor to enhance the growth of neurons in the presence of inhibitory chondroitin sulfate proteoglycans. Neurosci. Insights *18*, 26331055231186993. https://doi.org/10.1177/26331055231186993.
31. Sacchetti, P., Sousa, K.M., Hall, A.C., Liste, I., Steffensen, K.R., Theofilopoulos, S., Parish, C.L., Hazenberg, C., Richter, L.A., Hovatta, O., et al. (2009). Liver X receptors and oxysterols promote ventral midbrain neurogenesis in vivo and in human embryonic stem cells. Cell Stem Cell *5*, 409–419. https://doi.org/10.1016/j.stem.2009.08.019.
32. Theofilopoulos, S., Abreu de Oliveira, W.A., Yang, S., Yutuc, E., Saeed, A., Abdel-Khalik, J., Ullgren, A., Cedazo-Minguez, A., Björkhem, I., Wang, Y., et al. (2019). 24(S),25-Epoxycholesterol and cholesterol 24S-hydroxylase (CYP46A1) overexpression promote midbrain dopaminergic neurogenesis in vivo. J. Biol. Chem. *294*, 4169–4176. https://doi.org/10.1074/jbc.RA118.005639.
33. Theofilopoulos, S., Wang, Y., Kitambi, S.S., Sacchetti, P., Sousa, K.M., Bodin, K., Kirk, J., Saltó, C., Gustafsson, M., Toledo, E.M., et al. (2013). Brain endogenous liver X receptor ligands selectively promote midbrain neurogenesis. Nat. Chem. Biol. *9*, 126–133. https://doi.org/10.1038/nchembio.1156.
34. Wang, Y., Sousa, K.M., Bodin, K., Theofilopoulos, S., Sacchetti, P., Hornshaw, M., Woffendin, G., Karu, K., Sjövall, J., Arenas, E., and Griffiths, W.J. (2009). Targeted lipidomic analysis of oxysterols in the embryonic central

nervous system. Mol. Biosyst. *5*, 529–541. https://doi.org/10.1039/b819502a.

35. Yutuc, E., Dickson, A.L., Pacciarini, M., Griffiths, L., Baker, P.R.S., Connell, L., Öhman, A., Forsgren, L., Trupp, M., Vilarinho, S., et al. (2021). Deep mining of oxysterols and cholestenoic acids in human plasma and cerebrospinal fluid: Quantification using isotope dilution mass spectrometry. Anal. Chim. Acta *1154*, 338259. https://doi.org/10.1016/j.aca.2021.338259.

36. Yutuc, E., Angelini, R., Baumert, M., Mast, N., Pikuleva, I., Newton, J., Clench, M.R., Skibinski, D.O.F., Howell, O.W., Wang, Y., and Griffiths, W.J. (2020). Localization of sterols and oxysterols in mouse brain reveals distinct spatial cholesterol metabolism. Proc. Natl. Acad. Sci. USA *117*, 5749–5760. https://doi.org/10.1073/pnas.1917421117.

37. Nowakowski, R.S., Lewin, S.B., and Miller, M.W. (1989). Bromodeoxyuridine immunohistochemical determination of the lengths of the cell cycle and the DNA-synthetic phase for an anatomically defined population. J. Neurocytol. *18*, 311–318. https://doi.org/10.1007/BF01190834.

38. Janowski, B.A., Grogan, M.J., Jones, S.A., Wisely, G.B., Kliewer, S.A., Corey, E.J., and Mangelsdorf, D.J. (1999). Structural requirements of ligands for the oxysterol liver X receptors LXRalpha and LXRbeta. Proc. Natl. Acad. Sci. USA *96*, 266–271. https://doi.org/10.1073/pnas.96.1.266.

39. Lehmann, J.M., Kliewer, S.A., Moore, L.B., Smith-Oliver, T.A., Oliver, B.B., Su, J.L., Sundseth, S.S., Winegar, D.A., Blanchard, D.E., Spencer, T.A., and Willson, T.M. (1997). Activation of the nuclear receptor LXR by oxysterols defines a new hormone response pathway. J. Biol. Chem. *272*, 3137–3140. https://doi.org/10.1074/jbc.272.6.3137.

40. Willy, P.J., Umesono, K., Ong, E.S., Evans, R.M., Heyman, R.A., and Mangelsdorf, D.J. (1995). LXR, a nuclear receptor that defines a distinct retinoid response pathway. Genes Dev. *9*, 1033–1045. https://doi.org/10.1101/gad.9.9.1033.

41. Pehkonen, P., Welter-Stahl, L., Diwo, J., Ryynänen, J., Wienecke-Baldacchino, A., Heikkinen, S., Treuter, E., Steffensen, K.R., and Carlberg, C. (2012). Genome-wide landscape of liver X receptor chromatin binding and gene regulation in human macrophages. BMC Genom. *13*, 50. https://doi.org/10.1186/1471-2164-13-50.

42. Savory, J.G.A., Edey, C., Hess, B., Mears, A.J., and Lohnes, D. (2014). Identification of novel retinoic acid target genes. Dev. Biol. *395*, 199–208. https://doi.org/10.1016/j.ydbio.2014.09.013.

43. Durak, O., Gao, F., Kaeser-Woo, Y.J., Rueda, R., Martorell, A.J., Nott, A., Liu, C.Y., Watson, L.A., and Tsai, L.-H. (2016). Chd8 mediates cortical neurogenesis via transcriptional regulation of cell cycle and Wnt signaling. Nat. Neurosci. *19*, 1477–1488. https://doi.org/10.1038/nn.4400.

44. Marchetto, M.C., Belinson, H., Tian, Y., Freitas, B.C., Fu, C., Vadodaria, K., Beltrao-Braga, P., Trujillo, C.A., Mendes, A.P.D., Padmanabhan, K., et al. (2017). Altered proliferation and networks in neural cells derived from idiopathic autistic individuals. Mol. Psychiatry *22*, 820–835. https://doi.org/10.1038/mp.2016.95.

45. Mariani, J., Coppola, G., Zhang, P., Abyzov, A., Provini, L., Tomasini, L., Amenduni, M., Szekely, A., Palejev, D., Wilson, M., et al. (2015). FOXG1-Dependent Dysregulation of GABA/Glutamate Neuron Differentiation in Autism Spectrum Disorders. Cell *162*, 375–390. https://doi.org/10.1016/j.cell.2015.06.034.

46. Paulsen, B., Velasco, S., Kedaigle, A.J., Pigoni, M., Quadrato, G., Deo, A.J., Adiconis, X., Uzquiano, A., Sartore, R., Yang, S.M., et al. (2022). Autism genes converge on asynchronous development of shared neuron classes. Nature *602*, 268–273. https://doi.org/10.1038/s41586-021-04358-6.

47. Kim, N.-S., Ringeling, F.R., Zhou, Y., Nguyen, H.N., Temme, S.J., Lin, Y.-T., Eacker, S., Dawson, V.L., Dawson, T.M., Xiao, B., et al. (2022). CYFIP1 dosages exhibit divergent behavioral impact via diametric regulation of NMDA receptor complex translation in mouse models of psychiatric disorders. Biol. Psychiatry *92*, 815–826. https://doi.org/10.1016/j.biopsych.2021.04.023.

48. Silva, A.I., Kirov, G., Kendall, K.M., Bracher-Smith, M., Wilkinson, L.S., Hall, J., Ulfarsson, M.O., Walters, G.B., Stefansson, H., Stefansson, K., et al. (2021). Analysis of diffusion tensor imaging data from the UK biobank confirms dosage effect of 15q11.2 copy number variation on white matter and shows association with cognition. Biol. Psychiatry *90*, 307–316. https://doi.org/10.1016/j.biopsych.2021.02.969.

49. Sakakura, Y., Shimano, H., Sone, H., Takahashi, A., Inoue, N., Toyoshima, H., Suzuki, S., and Yamada, N. (2001). Sterol regulatory element-binding proteins induce an entire pathway of cholesterol synthesis. Biochem. Biophys. Res. Commun. *286*, 176–183. https://doi.org/10.1006/bbrc.2001.5375.

50. Wong, J., Quinn, C.M., Guillemin, G., and Brown, A.J. (2007). Primary human astrocytes produce 24(S),25-epoxycholesterol with implications for brain cholesterol homeostasis. J. Neurochem. *103*, 1764–1773. https://doi.org/10.1111/j.1471-4159.2007.04913.x.

51. Sodero, A.O. (2021). 24S-hydroxycholesterol: Cellular effects and variations in brain diseases. J. Neurochem. *157*, 899–918. https://doi.org/10.1111/jnc.15228.

52. Arai, Y., Pulvers, J.N., Haffner, C., Schilling, B., Nüsslein, I., Calegari, F., and Huttner, W.B. (2011). Neural stem and progenitor cells shorten S-phase on commitment to neuron production. Nat. Commun. *2*, 154. https://doi.org/10.1038/ncomms1155.

53. Parente, M., Tonini, C., Buzzelli, V., Carbone, E., Trezza, V., and Pallottini, V. (2022). Brain cholesterol biosynthetic pathway is altered in a preclinical model of fragile X syndrome. Int. J. Mol. Sci. *23*, 3408. https://doi.org/10.3390/ijms23063408.

54. Tomita, H., Hines, K.M., Herron, J.M., Li, A., Baggett, D.W., and Xu, L. (2022). 7-Dehydrocholesterol-derived oxysterols cause neurogenic defects in Smith-Lemli-Opitz syndrome. Elife *11*, e67141. https://doi.org/10.7554/eLife.67141.

55. Thurm, A., Tierney, E., Farmer, C., Albert, P., Joseph, L., Swedo, S., Bianconi, S., Bukelis, I., Wheeler, C., Sarphare, G., et al. (2016). Development, behavior, and biomarker characterization of Smith-Lemli-Opitz syndrome: an update. J. Neurodev. Disord. *8*, 12. https://doi.org/10.1186/s11689-016-9145-x.

56. Leoni, V., and Caccia, C. (2011). Oxysterols as biomarkers in neurodegenerative diseases. Chem. Phys. Lipids *164*, 515–524. https://doi.org/10.1016/j.chemphyslip.2011.04.002.

57. Björkhem, I. (2006). Crossing the barrier: oxysterols as cholesterol transporters and metabolic modulators in the brain. J. Intern. Med. *260*, 493–508. https://doi.org/10.1111/j.1365-2796.2006.01725.x.

58. Gamba, P., Testa, G., Sottero, B., Gargiulo, S., Poli, G., and Leonarduzzi, G. (2012). The link between altered cholesterol metabolism and Alzheimer's disease. Ann. N. Y. Acad. Sci. *1259*, 54–64. https://doi.org/10.1111/j.1749-6632.2012.06513.x.

59. Jin, U., Park, S.J., and Park, S.M. (2019). Cholesterol Metabolism in the Brain and Its Association with Parkinson's Disease. Exp. Neurobiol. *28*, 554–567. https://doi.org/10.5607/en.2019.28.5.554.

60. Karasinska, J.M., and Hayden, M.R. (2011). Cholesterol metabolism in Huntington disease. Nat. Rev. Neurol. *7*, 561–572. https://doi.org/10.1038/nrneurol.2011.132.

61. Sun, Z., Zhao, L., Bo, Q., Mao, Z., He, Y., Jiang, T., Li, Y., Wang, C., and Li, R. (2021). Brain-Specific Oxysterols and Risk of Schizophrenia in Clinical High-Risk Subjects and Patients With Schizophrenia. Front. Psychiatry *12*, 711734. https://doi.org/10.3389/fpsyt.2021.711734.

62. Grayaa, S., Zerbinati, C., Messedi, M., HadjKacem, I., Chtourou, M., Ben Touhemi, D., Naifar, M., Ayadi, H., Ayedi, F., and Iuliano, L. (2018). Plasma oxysterol profiling in children reveals 24-hydroxycholesterol as a potential marker for Autism Spectrum Disorders. Biochimie *153*, 80–85. https://doi.org/10.1016/j.biochi.2018.04.026.

63. Guidara, W., Messedi, M., Maalej, M., Naifar, M., Khrouf, W., Grayaa, S., Maalej, M., Bonnefont-Rousselot, D., Lamari, F., and Ayadi, F. (2021). Plasma oxysterols: Altered level of plasma 24-hydroxycholesterol in

patients with bipolar disorder. J. Steroid Biochem. Mol. Biol. *211*, 105902. https://doi.org/10.1016/j.jsbmb.2021.105902.

64. Cardo, L.F., de la Fuente, D.C., and Li, M. (2023). Impaired neurogenesis and neural progenitor fate choice in a human stem cell model of SETBP1 disorder. Mol. Autism. *14*, 8. https://doi.org/10.1186/s13229-023-00540-x.
65. Writing Committee for the ENIGMA-CNV Working Group; Sønderby, I.E., Sønderby, I.E., Kaufmann, T., Walters, G.B., Abdellaoui, A., Ames, D., Amunts, K., Andersson, M., Armstrong, N.J., et al. (2020). Association of Copy Number Variation of the 15q11.2 BP1-BP2 Region With Cortical and Subcortical Morphology and Cognition. JAMA Psychiatr. *77*, 420–430. https://doi.org/10.1001/jamapsychiatry.2019.3779.
66. Sunner, K., and Pullen, A.H. (1995). Phosphorylated neurofilament antigen redistribution in intercostal nerve subsequent to retrograde axonal transport of diphtheria toxin. Acta Neuropathol. *89*, 331–340. https://doi.org/10.1007/BF00309626.
67. Darnell, J.C., Van Driesche, S.J., Zhang, C., Hung, K.Y.S., Mele, A., Fraser, C.E., Stone, E.F., Chen, C., Fak, J.J., Chi, S.W., et al. (2011). FMRP stalls ribosomal translocation on mRNAs linked to synaptic function and autism. Cell *146*, 247–261. https://doi.org/10.1016/j.cell.2011.06.013.
68. Sawicka, K., Hale, C.R., Park, C.Y., Fak, J.J., Gresack, J.E., Van Driesche, S.J., Kang, J.J., Darnell, J.C., and Darnell, R.B. (2019). FMRP has a cell-type-specific role in CA1 pyramidal neurons to regulate autism-related transcripts and circadian memory. Elife *8*, e46919. https://doi.org/10.7554/eLife.46919.
69. Ascano, M., Mukherjee, N., Bandaru, P., Miller, J.B., Nusbaum, J.D., Corcoran, D.L., Langlois, C., Munschauer, M., Dewell, S., Hafner, M., et al. (2012). FMRP targets distinct mRNA sequence elements to regulate protein expression. Nature *492*, 382–386. https://doi.org/10.1038/nature11737.
70. Zhao, S., Maxwell, S., Jimenez-Beristain, A., Vives, J., Kuehner, E., Zhao, J., O'Brien, C., de Felipe, C., Semina, E., and Li, M. (2004). Generation of embryonic stem cells and transgenic mice expressing green fluorescence protein in midbrain dopaminergic neurons. Eur. J. Neurosci. *19*, 1133–1140. https://doi.org/10.1111/j.1460-9568.2004.03206.x.
71. Yu, G., Wang, L.-G., Han, Y., and He, Q.-Y. (2012). clusterProfiler: an R package for comparing biological themes among gene clusters. OMICS *16*, 284–287. https://doi.org/10.1089/omi.2011.0118.
72. Crick, P.J., William Bentley, T., Abdel-Khalik, J., Matthews, I., Clayton, P.T., Morris, A.A., Bigger, B.W., Zerbinati, C., Tritapepe, L., Iuliano, L., et al. (2015). Quantitative charge-tags for sterol and oxysterol analysis. Clin. Chem. *61*, 400–411. https://doi.org/10.1373/clinchem.2014.231332.

STAR★METHODS

KEY RESOURCES TABLE

REAGENT or RESOURCE	SOURCE	IDENTIFIER
Antibodies		
CTIP2	Abcam	Cat# AB18465; RRID:AB_2064130
FOXG1	Abcam	Cat# AB18259; RRID:AB_732415
Ki67	BD Pharmingen	Cat# 550609; RRID:AB_393778
NESTIN	Millipore	Cat# ABD69; RRID:AB_2744681
NeuN	Millipore	Cat# MAB377; RRID:AB_2298772
NeuN	Millipore	Cat# ABN78; RRID:AB_10807945
$P27^{KIP1}$	Millipore	Cat# 06–445; RRID:AB_310121
PAX6	DSHB	Cat# pax6; RRID:AB_528427
pH3	BioLegend	Cat# 641002; RRID:AB_1227659
SATB2	Abcam	Cat# AB51502; RRID:AB_882455
TBR1	Abcam	Cat# AB31940; RRID:AB_2200219
CYFIP1	Millipore	Cat# AB6046; RRID:AB_10807712
GAPDH	Abcam	Cat# AB8245; RRID:AB_2107448
GAPDH	Abcam	Cat# AB9485; RRID:AB_307275
NIPA1	Abcam	Cat# AB128640; RRID:AB_11141454
NIPA2	Abcam	Cat# AB84343; RRID:AB_1925251
TUBGCP5	Abcam	Cat# AB168325
LXRB	Novus Biologicals	Cat# NB100-74457; RRID:AB_1049252
Chemicals, peptides, and recombinant proteins		
DMEM/F12	ThermoFisher Scientific	Cat# 11330-032
Matrigel	Corning	Cat# CB40230
mTeSR1	Stem Cell Technologies	Cat# 85850
Y-27632	Reprocell	Cat# 04-0012-10
Accutase	ThermoFisher Scientific	Cat# 00-4555-56
N2	ThermoFisher Scientific	Cat# 17502048
B27 Supplement minus retinoid	ThermoFisher Scientific	Cat# 12587010
B27 Supplement	ThermoFisher Scientific	Cat# 17504044
SB431542	Tocris	Cat# 1614
LDN-193189	StemGen	Cat# 1062368-24-4
Laminin	ThermoFisher Scientific	Cat# 23017–015
DAPI	ThermoFisher Scientific	Cat# 62248
Puromycin	ThermoFisher Scientific	Cat# A1113803
DMSO	Sigma-Aldrich	Cat# D2650
RIPA buffer	Abcam	Cat# Ab156034
NuPAGE™ LDS Sample Buffer	ThermoFisher Scientific	Cat# NP0007
NuPAGE™ Sample Reducing Agent	ThermoFisher Scientific	Cat# NP0004
Critical commercial assays		
P3 4D nucleofection kit	Lonza	Cat# V4XP-3024
SYBR Green Master Mix	ThermoFisher Scientific	Cat# F416L
Click-iT™ Plus EdU Cell Proliferation Kit	ThermoFisher Scientific	Cat# C10637
CytoTune®-iPS 2.0 Sendai Reprogramming Kit	ThermoFisher Scientific	Cat# A16518
Lipofectamine® RNAiMAX transfection reagent	ThermoFisher Scientific	Cat# 13778500
Hyperprep KAPA kit	Roche	Cat# KR0961 – v7.19

(*Continued on next page*)

Continued

REAGENT or RESOURCE	SOURCE	IDENTIFIER
24R/S-hydroxycholesterol-D6	SigmaAldrich	Cat # 700018P
7α-hydroxycholesterol-D7	SigmaAldrich	Cat # LM-4103
7-oxocholesterol-D7	SigmaAldrich	Cat # LM-4107
22S-3O-hydroxycholesterol-D7	SigmaAldrich	Cat # 700051P
7α, 25-dihydroxycholsterol-D6	SigmaAldrich	Cat # 700078
3β-hydroxycholest-5-en-26-oic acid-D5	SigmaAldrich	Cat # 700151P
7αH,3O-hydroxycholestenoic acid-D3	SigmaAldrich	Cat # 700194P
Desmosterol-D6	SigmaAldrich	Cat # 700040P
Cholesterol-D7	SigmaAldrich	Cat # 700041P
24(S),25-Epoxycholesterol	Abcam	Cat# ab141633
Deposited data		
RNA sequencing of PSC-derived neural cells	This paper	GEO: GSE119316
Experimental models: Cell lines		
H7	WiCell	Cat# WA07; RRID:CVCL_9772
CYFIP1-GoF	This paper	N/A
iCas9	Huangfu D laboratory, ref. 21	N/A
CYFIP1-LoF	This paper	N/A
LXRb KO	This paper	N/A
202	This paper	N/A
900	This paper	N/A
EA8	This paper	N/A
EA62	This paper	N/A
Recombinant DNA		
CYFIP1 ORF	OriGene	Cat# SC100426
pCAG-IRES-PAC	This paper	N/A
pCAG-CYFIP1-IRES-PAC	This paper	N/A
pGEM-T Easy	Promega	Cat# A1360
Software and algorithms		
FlowJo_V10	www.flowjo.com	RRID:SCR_008520
ImageJ	NIH	RRID:SCR_003070
CellProfiler	www.cellprofiler.org	RRID:SCR_007358
R packages	www.r-pkgs.org/	RRID:SCR_003005
Bioconductor Packages	www.bioconductor.org	RRID:SCR_006442
TraceFinder 5.1	ThermoFisher Scientific	RRID:SCR_023045

RESOURCE AVAILABILITY

Lead contact

Further information and requests for resources and reagents should be directed to and will be fulfilled by the lead contact, Meng Li. lim26@cf.ac.uk.

Materials availability

All unique reagents generated in this study are available from the lead contact with a completed materials transfer agreement.

Data and code availability

The raw sequencing data can be downloaded from the GEO website through the accession number GSE119316. Pipelines for the cell cycle analysis can be downloaded from https://github.com/DanCF93/delafuente_et_al_2024. Access to additional information generated in this study can be obtained upon request from the lead contact.

EXPERIMENTAL MODEL AND SUBJECT DETAILS

Generation of CYFIP1-GoF and CYFIP1-LoF PSC lines by transgene expression and CRISPR/Cas9 assisted genome editing

The CYFIP1 overexpression (CYFIP1-GoF) lines were generated on H7 background (WiCell). The CYFIP1 loss-of-function (CYFIP1-LoF) lines were engineered using the iCas9 as the parental line,[21] which contains a doxycycline inducible Cas9 expression cassette for increasing the genome editing efficiency.

For making the CYFIP1-GoF lines, human CYFIP1 open reading frame (SC100426, OriGene) was cloned into a pCAG-IRES-PAC plasmid upstream of the IRES sequence.[70] The resulting pCAG-CYFIP1-IRES-PAC vector was transfected into H7 hESCs using the 4D-Nucleofector system (Lonza). Stable H7 transfectants were selected by Puromycin (1μg/mL, Sigma) for 10 days prior to colony picking and clonal expansion. CYFIP1 expression was validated by RT-PCR and Western blot analysis (Figure S1). Two clones (#3 and #5) that exhibit approximately 2-fold CYFIP1 protein level to that of the parental control H7 cells were used for this study.

For generating CYFIP1-LoF cells, guide RNAs (gRNAs) were designed to target the first coding exon, common to 6 of 7 isoforms of the *CYFIP1* gene (gRNA1 5′- GGAGGACGCGCTGTCCAACG -3′, gRNA2 5′- TGCAGGGCTGCTGGTCGGGC-3′, gRNA2 5′- GTCACC TGGGCCGCCATCCT-3′). All gRNAs were synthesized as RNAs by *in vitro* transcription and transfected into iCas9 hESCs using Lipofectamine RNAiMAX. Briefly, gRNA and ssDNA were added at a 10 nM and 20 nM final concentration, respectively. gRNAs and Lipofectamine RNAiMAX were diluted separately in Opti-MEM, mixed together, incubated for 5 min at RT, and added dropwise to cultured hPSCs. 110 individual colonies were picked from day 10 post transfection and clonally expanded while the remaining pool of transfected cells were used for Surveyor Assay (Integrated DNA Technologies). Genomic DNA was collected for each clone and the targeted region was screened by PCR of genomic DNA using two pairs of primers: Forward 1, 5′-ATGTGTTGTTCCAGCC CAGG-3′, Reverse 1 5′-CATCATGTGGGGTCGGAGC-3′, which give rise to a predicted 190bp product. Forward 2 5′-CCCTGAGA GAGACACGCAAC-3′, Reverse 1 5′-CCTCACTGCATAGTCTATTGGGA-3′, which give rise to a 557bp product. PCR products suggesting deletions and insertions (INDELs) were then confirmed by cloning into a pGEM-T Easy vector (Promega) followed by Sanger sequencing (GATC Biotech). CYFIP1 protein levels of confirmed targeted cells were validated by Western blot analysis.

iPSC reprograming and quality control analysis

Fibroblasts from two adult male subjects carrying 15q11.2 deletion and two adult healthy subjects (one male and one female) were reprogrammed into induced pluripotent stem cells (iPSCs) using the CytoTune-IPS 2.0 Sendai reprogramming kit (ThermoFisher). Multiple clones were obtained for each carrier and two clones each were used in this study (EA8.4, EA8.21, EA62.13 and EA62.19). The iPSC lines, the genome edited hESC lines and their isogenic control lines used in this study were regularly tested for mycoplasma contamination. Genome wide screen was performed for potential inadvertent genomic event occurred during reprograming and/or CRISPR/Cas9 genome editing using the Infinium Psych Array v1.1. The iScan data were uploaded to the Illumina Genome Studio v2.0.4 and call rate threshold set at 0.95. Datasets were analyzed using the PennCNV software (http://penncnv.openbioinformatics.org). Quality controls steps included merging of CNVs with between CNV fraction of <0.2 (<20%), and exclusion of those <100,000 bp in length and containing <10 single nucleotide polymorphisms (SNPs). Log R ratio and B allele frequency plots were generated for each CNV and checked for reliability of the call. The screening outcome is provided in Table S11.

Generation and genetic manipulation of human iPSC were approved by Cardiff University and HSE (GMO130/669). Collection of human skin biopsies and reprograming was approved by the Regional Ethics Committee of the National Health Service (study 14/WA/0035).

METHOD DETAILS

Stem cell culture and differentiation

All hPSCs were cultured on Matrigel coated plates in E8 media (ThermoFisher). Media was changed daily, and cells passaged mechanically with 0.02% EDTA at 80% confluence. Cortical neuronal differentiation was performed using method described by Cardo et al.[64] Briefly, PSCs from 80% confluent wells of a 6-well plate were plated onto a 12-well plate previously coated with reduced growth factor Matrigel (VWR) in E8 media (d0) and changed to retinoid free N2B27 the next day. For the first 10 days, cultures were supplemented with SB431542 (10μM, Tocris) and LDN-193189 (100nM, Tocris). During differentiation, the cultures were split twice using EDTA. The first split was done *en bloc* onto fibronectin-coated plates at approximately d10 and the second split to single cells onto poly-D-lysine/laminin-coated coverslips at around d20. Retinol free B27 was switched to standard B27 on d20 to aid neuronal maturation. For oxysterol experiments, 24S, 25-epoxycholesterol (1-10μM, Abcam) or ethanol control were added to N2B27 media for 10 days either during d15–25 or d20-30.

RNAseq and LCMS experiments were performed using GoF #5 and LoF#31 and respective isogenic controls. Neuronal differentiations examined by immunocytochemical staining and flow cytometry were performed with two independent CYFIP1 manipulated lines with their respective isogenic control lines. Unless indicated otherwise, two differentiation runs (n = 2) were performed with the GoF #5 and LoF#31 plus one repeat using GoF #3 and LoF#41, respectively. IPSC experiments were carried out using two clones each of the two 15q11.2del iPSC lines and two control iPSC lines in every differentiation run. Additional information on cell line used is provided in Table S10.

Immunocytochemistry

Cultures were fixed with 3.7% PFA for 15–20 min at 4°C. For nuclear antigen detection an additional fixation with methanol gradient was performed, which includes 5 min each in 33% and 66% methanol at room temperature followed by 100% methanol for 20 min at −20. Cultures were then returned to PBST via inverse gradient and were then permeabilized with three 10-min washes in 0.3% Triton X-100 solution in PBS (PBS-T) and then blocked in PBS-T containing 3% BSA and 5% donkey serum. Cells were incubated with primary antibodies in blocking solution overnight at 4°C. Following three PBS-T washes, Alexa-Fluor secondary antibodies were added at 1:2000 in PBS-T for 1 h at ambient temperature in the dark. Three PBS washes were then performed that included once with DAPI at 1:3000 Images were taken on a PerkinElmer OperaPhenix or a Leica DMI6000B inverted microscope. Quantification was carried out in Cell Profiler (cellprofiler.org) or manually using ImageJ (imagej.net) by examining 10 randomly selected field of views from each of the 3 technical replicates performed in at least 3 independent differentiations (biological replicates). The antibodies used are provided in the key resource table.

EdU labeling and detection

Cells in S-phase were labeled using the Click-iT EdU Assay kit. For EdU-pulse analysis, cells were incubated with EdU for 2 h at specified day of differentiation. For EdU- cumulative assay required for calculating cell cycle length, cells were incubated for increasing periods of time of 2, 4, 8, 16, 24 and 48 h. Cells were then fixed in 3.7% PFA for 15 min at 4°C. EdU detection was carried out as per manufacturer's protocol. Cell cycle length determination was performed using the Nowakowski equation. Nine fields each from 3 technical replicates and 3 independent differentiations were counted at each time point of the EdU cumulative labeling. The percentages of EdU^+ in ethanol and 24S,25-EC conditions were plotted against time. A linear regression was performed, and the values of the slope (m) and y-intercept (b) of the linear equation were used to calculate the values of cell cycle length (tc) and S-phase length (ts), using the Nowakowski equation:

GF(t) = (GF/tc)t + GF(ts/tc). Where: GF = Growth fraction in cell population, m = GF/tc thus tc = GF/m, b = GF(ts/tc) thus ts=(b*tc)/GF.

Flow cytometry

Cultured cells were dissociated in Accutase (ThermoFisher) for 10 min at 37°C, then washed and counted. Samples containing 10^6 cells were fixed in 70% EtOH for 2 h at 4°C. The cells were washed in DPBS and incubated with DAPI (0.3 μg/mL) and of RNaseA (200 μg/mL) for 30 min. The samples were analyzed on a BD LSRFortessa cell analyser (BD Biosciences). Results were analyzed using FLOWJO software. Statistical analysis was performed in R (www.r-project.org).

Quantitative PCR

Total RNA was extracted using TRI reagent (Sigma) according to the manufacturer's instructions. Reverse transcription was performed using SS RTIII (Invitrogen). QPCR was carried out using SYBR MESA green on a BioRad CFX connect system. All data were normalised to three reference genes (*GAPDH, b-ACTIN*). The sequence information for PCR primers are provided below. All qPCR data are presented as mean ± s.e.m. of biological duplicates or triplicates. The Primers used for qPCR were: IRES Forward 5′-CCACCATATTGCCGTCTT-3′, IRES Reverse 5′-GAGGAACTGCTTCCTTCA-3'; CYFIP1 Forward 5′-GAAAACCGTGGAGGT TCTGGA-3′, CYFIP1 Reverse 5′-GCTCAATGGCATTTCTCTGGAAG-3'; GAPDH Forward 5′- ATGACATCAAGAAGGTGGTG-3′, GAPDH Reverse 5′- CATACCAGGAAATGAGCTTG-3'; β-Actin Forward 5′- TCACCACCACGGCCGAGCG-3′, β-Actin Reverse 5′- TCTCCTTCTGCATCCTGTCG.

RNA extraction and bulk RNA sequencing

The cell lines used for this experiment were CYFIP1-GoF #5 and isogenic control H7, CYFIP1-LoF#31 and isogenic control iCas9, EA08 #4 and EA62 #13 and control iPSC 900. Three biological replicates were produced for each cell line and time-points of differentiation. Total RNA was extracted from TRIzol lysates using the PureLink RNA mini kit (ThermoFisher). RNA integrity was analyzed using the RNA 6000 nano chip for the Agilent Bioanalyzer 2100 and only samples with a RIN >9 were used for sequencing. The mRNA Hyperprep KAPA kit (Roche) was used for isolating mRNA and constructing the mRNA libraries. Indexed samples were pooled together and sequenced on an Illumina HiSeq 4000 (Illumina, San Diego, USA). Paired-end sequencing and a depth of approximately 33 million reads per sample were used for all sequencing experiments.

Analysis of RNA sequencing data

FASTQ files were trimmed and mapped to the Ensembl human genome GRCh38.84 (hg38) using STAR 2.5.1b.65. Quality of the samples was assessed using FastQC (v 0.11.2) prior and after trimming. Gene counts were obtained using the Samtools Feature count command. Library size normalisation and differential gene expression was carried out using the R/Bioconductor package DESeq2. Genes with less than 10 counts in at least one of the replicates were excluded from the analysis. Subsequent study of the DEGs was performed on protein-coding Entrez genes with a Benjamini Hochberg-corrected $p < 0.05$. The R/Bioconductor package clusterProfiler[71] was used to identify GO terms enriched in DEGs when compared to a background set consisting of all protein-coding genes expressed in the cell-line at that developmental stage. To remove highly similar GO terms, semantic similarity between terms

was calculated following the method described in clusterProfiler (https://yulab-smu.top/biomedical-knowledge-mining-book/semantic-similarity-overview.html). Terms with a threshold over 0.7 were removed keeping the term with the smallest p value.

Western Blot

Cultured cells were lysed on ice using RIPA buffer (Abcam) supplemented with protease and phosphatase inhibitors (Sigma). Cell lysates were centrifuged for 15 min at 12000g and the resulting supernatant was combined with 1X Bolt LDS Sample Buffer (ThermoFisher) and 1X Bolt Sample Reducing Agent (ThermoFisher) and boiled at 97°C for 5 min. Equal amounts of proteins for each sample were separated on 4–12% Bolt Bis-Tris Plus gels (ThermoFisher) and then transferred to a PVDF membrane (0.45 μm pore size, Amersham Hybond, GE Healthcare) via electro-blotting. The membrane was blocked in 5% BSA (Sigma) and incubated with primary antibodies overnight at 4°C. The membrane was then washed in TBS-T (Tris-Buffered Saline containing 0.1% Tween 20). Secondary antibodies were incubated for 2 h at room temperature. The membranes were imaged in an Odyssey CLx Imaging system (LI-COR) or in a Gel Doc XR system (Bio-Rad). The antibodies used are provided in the key resource table.

Sterol extraction, derivatization and LC-MS

Sterols were extracted from cell pellet through the dropwise addition of 1mL ethanol containing the internal standards under sonication in an ultrasonic bath. Samples were then centrifuged at 16,000g (13,000rpm) @ 4°C for 30mins. Supernatant was then collected and diluted with water to give a 70% ethanol solution. Oxysterols were separated from cholesterol by C18 solid-phase extraction and derivatized with Girard P reagent (TCI Europe) with or without prior oxidation of 3β-hydroxy to 3-oxo groups as previously described in detail.[35,72] Samples were analyzed by LC-MS(MSn) on an UltiMate 3000 Micro LC system coupled to an Orbitrap ID-X mass spectrometer (Thermo Fisher Scientific). Chromatographic separation was performed using a Hypersil Gold RP column (50 × 2.1 mm, 1.9 μm, Thermo Fisher Scientific). Mass spectra were recorded at high resolution in the Orbitrap analyzer, and MSn spectra recorded simultaneously in the ion-trap. Quantification was performed by stable isotope dilution on reconstructed ion-chromatograms generated in the Orbitrap using TraceFinder 5.1 software (Thermo Fisher Scientific). Isotope-labelled internal standards were purchased from Avanti Polar Lipids Inc (AL, USA), including 24R/S-hydroxycholesterol-D6 (cat # 700018P), 7α-hydroxycholesterol-D7 (cat # LM-4103), 7-oxocholesterol-D7 (cat # LM-4107), 22S-3O-hydroxycholesterol-D7 (cat # 700051P), 7α, 25-dihydroxycholsterol-D6 (cat # 700078), 3β-hydroxycholest-5-en-26-oic acid-D5 (cat # 700151P), 7αH,3O-hydroxycholestenoic acid-D3 (cat # 700194P), desmosterol-D6 (cat # 700040P) and cholesterol-D7 (cat # 700041P). The identification of 24S,24-EC is based on the accurate mass of parent ions (≤5 ppm) and MS3 fragmentation spectrum which are matched to the authentic standard.

QUANTIFICATION AND STATISTICAL ANALYSES

All data were collected from at least three independent experiments and presented as mean ± s.e.m. unless otherwise specified (Table S10). Data were tested for normality with the Shapiro-Wilk test and for equal variance with Levene test before performing statistical analyses by *t* test or ANOVA as stated in the figure legends where relevant. Post-hoc Tukey test was applied following ANOVA for multiple comparisons. All statistical tests were performed in R (www.r-project.org).